NASA TECHNICAL MEMORANDUM


NASA TM X-3358

NASA TM X-3358

# BOUNDARY-LAYER BLEED SYSTEM STUDY FOR A FULL-SCALE, MIXED-COMPRESSION INLET WITH 45 PERCENT INTERNAL CONTRACTION

*Robert J. Shaw, Joseph F. Wasserbauer, and Harvey E. Neumann*

*Lewis Research Center*
*Cleveland, Ohio 44135*


NATIONAL AERONAUTICS AND SPACE ADMINISTRATION • WASHINGTON, D. C. • MARCH 1976

| 1. Report No. | 2. Government Accession No. | 3. Recipient's Catalog No. |
|---|---|---|
| NASA TM X-3358 | | |

| 4. Title and Subtitle | 5. Report Date |
|---|---|
| BOUNDARY-LAYER BLEED SYSTEM STUDY FOR A FULL-SCALE, MIXED-COMPRESSION INLET WITH 45 PERCENT INTERNAL CONTRACTION | March 1976 |
| | 6. Performing Organization Code |

| 7. Author(s) | 8. Performing Organization Report No. |
|---|---|
| Robert J. Shaw, Joseph F. Wasserbauer, and Harvey E. Neumann | E-8494 |
| | 10. Work Unit No. 505-04 |
| 9. Performing Organization Name and Address | 11. Contract or Grant No. |
| Lewis Research Center<br>National Aeronautics and Space Administration<br>Cleveland, Ohio 44135 | |
| | 13. Type of Report and Period Covered |
| 12. Sponsoring Agency Name and Address | Technical Memorandum |
| National Aeronautics and Space Administration<br>Washington, D.C. 20546 | 14. Sponsoring Agency Code |

15. Supplementary Notes

16. Abstract

The results of an experimental bleed development study for a full-scale, Mach 2.5, axisymmetric, mixed-compression inlet are presented. The inlet was designed to satisfy the airflow requirements of the TF30-P-3 turbofan engine. Capabilities for porous bleed on the cowl surface and ram-scoop/flush-slot bleed on the centerbody were provided. A configuration with no bleed on the cowl achieved a minimum stable, diffuser exit, total pressure recovery of 0.894 with a centerbody-bleed mass flow ratio of 0.02. Configurations with cowl bleed had minimum stable recoveries as high as 0.900 but suffered range decrement penalties from the increased bleed mass flow removal. Limited inlet stability and unstart angle-of-attack data are presented.

| 17. Key Words (Suggested by Author(s)) | 18. Distribution Statement |
|---|---|
| Air intakes<br>Supersonic cruise inlets<br>Inlet bleed<br>Propulsion systems | Unclassified - unlimited<br>STAR Category 02 (rev.) |

| 19. Security Classif. (of this report) | 20. Security Classif. (of this page) | 21. No. of Pages | 22. Price* |
|---|---|---|---|
| Unclassified | Unclassified | 71 | $4.25 |

* For sale by the National Technical Information Service, Springfield, Virginia 22161

# BOUNDARY-LAYER BLEED SYSTEM STUDY FOR A FULL-SCALE, MIXED-COMPRESSION INLET WITH 45 PERCENT INTERNAL CONTRACTION

by Robert J. Shaw, Joseph F. Wasserbauer, and Harvey E. Neumann

Lewis Research Center

## SUMMARY

An experimental bleed development study for a full-scale, axisymmetric, mixed-compression inlet was conducted. The inlet was designed to satisfy the airflow requirements of the TF30-P-3 turbofan engine for Mach 2.5 operation. Capabilities for porous bleed on the cowl surface and ram-scoop/flush-slot bleed on the centerbody surface were provided. At the design Mach number, 55 percent of the supersonic area contraction occurred external to the cowl lip. Data were obtained at the design Mach number of 2.5 with a corresponding Reynolds number of 8.2 million per meter. Limited inlet stability and angle-of-attack data were also obtained.

The no-cowl-bleed configuration had the best range. The cowl-bleed configurations suffered range decrements of 48 to 122 kilometers (26 to 66 n mi) (relative to the no-cowl-bleed configuration.) The no-cowl-bleed configuration achieved a minimum stable, diffuser exit recovery of 0.894 with a centerbody-bleed mass flow ratio of 0.02. The cowl-bleed configurations had minimum stable recoveries to 0.900 for total bleed mass flow ratios to 0.055. Increasing centerbody-bleed flow to a maximum increased steady-state stability margins over the normal subcritical operating limits. If a constant centerbody-bleed plenum pressure were maintained, reductions in diffuser exit corrected airflow could be tolerated prior to unstart. These reductions ranged from 4.1 percent for the no-cowl-bleed configuration to 11.8 percent for the maximum-cowl-bleed configuration. Diffuser exit recoveries were slightly higher when the centerbody-bleed entrance used was a flush slot rather than a ram scoop.

The test results indicate that a nominally no-cowl-bleed configuration having cowl-bleed capability for off-design operation is the truely optimum bleed configuration (from the standpoints of inlet range and stability). With a centerbody-bleed flow of 0.02, the no-cowl-bleed configuration achieved a maximum angle of attack of $2.55^{\circ}$. With an increased centerbody-bleed flow, the configuration achieved a $6.85^{\circ}$ angle of attack prior to unstart. The various cowl-bleed configurations achieved still higher angles of attack for the respective operating conditions.

## INTRODUCTION

Efficient operation over the entire flight Mach number range is a fundamental design criterion of any aircraft inlet. For flight Mach numbers exceeding 2, mixed-compression inlets appear to offer the designer higher performance levels than comparable all-external-compression inlets. A properly designed mixed-compression inlet should provide high total pressure recovery and low total pressure distortion levels and incur low drag penalties. A critical area of design of any mixed-compression inlet is the internal boundary-layer bleed system. In particular, proper selection of not only the locations but also the amounts of airflow removal can significantly affect inlet performance from the standpoints of recovery, distortion, and drag. For an axisymmetric inlet, bleed flow removal is usually required on both the cowl and centerbody surfaces to maintain shock - boundary-layer control. In addition, sufficient subcritical corrected airflow stability margins are also required to avoid inlet unstarts from such internal disturbances as afterburner hardlights or sudden throttle movements. The inlet must also be tolerant to such external disturbances as gusts, and this tolerance can be achieved through a separate stability bleed system. Such a system is not discussed herein. However, increases in the amount of bleed airflow removal result in corresponding increases in bleed drag penalty suffered by the inlet; and such increases in drag can more than offset any increases in performance of the inlet. Thus, an optimized bleed system is a necessary part of any high-performance inlet design.

The study reported herein was conducted to determine such an optimum bleed system for an axisymmetric, mixed-compression inlet designed for operation at a flight Mach number of 2.5. At the design Mach number, approximately 55 percent of the supersonic area contraction occurred external to the cowl lip. The inlet was designed to provide the maximum external compression compatible with high total pressure recovery and low cowl drag. The inlet was sized to meet the airflow demands of the Pratt & Whitney TF30-P-3 turbofan engine at the design Mach number. The inlet-engine combination was to be used in an experimental propulsion system compatibility program to be conducted in the Lewis Research Center's 10- by 10-Foot Supersonic Wind Tunnel.

The bleed study reported herein was conducted in the 10- by 10-Foot Supersonic Wind Tunnel at a free-stream Mach number of 2.5 and at a Reynolds number of 8.2 million per meter. Test results are presented in the form of flow surveys made

at various positions within the inlet and as measurements of bleed flow rates, total pressure recoveries, and engine face distortion levels. Limited unstart angle-of-attack performance data are included.

U.S. customary units were used in the design of the test model and for recording and computing the experimental data. These units were converted to the International System of Units (SI) for presentation in this report.

## SYMBOLS

| | |
|---|---|
| $A$ | flow area, $m^2$ |
| $A_c$ | cowl-lip capture area (0.7073 $m^2$) |
| $d$ | distance from surface, cm |
| $H$ | annulus or rake height, cm |
| $L$ | centerbody support strut length, cm |
| $M$ | Mach number |
| $m/m_0$ | mass flow ratio |
| $P$ | total pressure, $N/m^2$ |
| $p$ | static pressure, $N/m^2$ |
| $R$ | cowl-lip radius (0.4745 m) |
| $r$ | radius, m |
| $W$ | cowl-bleed exit height, cm |
| $x$ | axial coordinate, m |
| $\alpha$ | angle of attack, deg |
| $\theta_l$ | cowl-lip position parameter, $\theta_l = \arctan (R/x)_{\text{Cowl lip}} = 26.4^o$ |
| $\varphi$ | circumferential rake position (counterclockwise looking downstream), deg |

Subscripts:

| | |
|---|---|
| ac | aft-cowl bleed |
| bl | bleed |

by bypass

cb centerbody bleed

fc forward-cowl bleed

max maximum

min minimum

x value at distance x

0 free stream

2 diffuser exit

Superscript:

$\bar{}$ area-weighted average

## APPARATUS AND PROCEDURE

### Inlet Model

The model used in this investigation was a full-scale inlet sized to meet the airflow demands of the TF30-P-3 turbofan engine at a free-stream Mach number of 2.5. It was a mixed-compression design with 55 percent of the supersonic area contraction occurring external to the cowl lip. Model hardware was designed to simulate the external contours and operating systems of a flight inlet system whenever possible. Internal contours were considered appropriate for an operational inlet system.

The inlet model is shown installed in the 10- by 10-Foot Supersonic Wind Tunnel in figure 1(a). For this investigation, the inlet was coupled to a cold-pipe - choked-exit-plug assembly. A nacelle cutaway illustrating the cold-pipe installation is shown in figure 1(b).

At the design Mach number of 2.5 and a free-stream temperature of 390 K, the TF30-P-3 requires a corrected airflow of 65.8 kg/sec (145 lb/sec). The inlet capture area was 0.7073 square meter. For these conditions, the engine required 93 percent of the capture mass flow at a total pressure recovery of 91.5 percent. Of the remaining inlet mass flow, 5.5 percent was allotted for performance bleed and 1.0 percent for overboard bypass flow for terminal-shock-position control. An additional 0.5 percent was spilled over the cowl.

Essential features of the inlet design are shown in isometric form in figure 1(c). The inlet centerbody had a two-cone spike with an initial cone half-angle of $12.5^{\circ}$ and a second cone half-angle of $18.5^{\circ}$. The design cowl-lip position parameter $\theta_l$ was $26.4^{\circ}$. The cowl lip had a leading-edge radius of 0.038 centimeter. The initial internal cowl angle was $2^{\circ}$ (from the centerline axis); the external cowl angle was set at $5^{\circ}$ to keep the cowl drag at a low value. Capability was provided for cowl bleed both forward and aft of the geometric throat and for centerbody bleed forward of the geometric throat.

The centerbody was supported by four equally spaced hollow struts. The centerbody-bleed flow was ducted overboard through these struts. Internal valves in each strut were used to control the centerbody-bleed flow. Cowl-bleed flows were discharged directly overboard. Overboard-bypass doors were used for terminal shock control. The inlet was started by translating the centerbody. A flight version of this inlet would require a collapsing centerbody (second cone) for starting and off-design operation.

The internal contours of the supersonic diffuser were determined from the inviscid method-of-characteristics analysis discussed in reference 1. The design philosophy was similar to that used to design the inlet of reference 2. The intent was to provide the maximum external compression compatible with high total pressure recovery and relatively low cowl drag and thus to reduce the length of the supersonic diffuser from the cowl lip to the geometric throat. A reduction in supersonic diffuser length would hopefully result in a decrease in the required cowl-bleed flow. The inlet was designed such that the isentropic compression fan from the internal surface of the cowl and the cowl-lip oblique shock were nearly focused on the centerbody surface. The compression was canceled at the centerbody with a sharp turn followed by an isentropic compression contour of the local surface as specified by the inviscid analysis. A centerbody-bleed slot was provided over this compression region for boundary-layer control just ahead of the geometric throat. It should be noted that the inviscid method-of-characteristics analysis did not account for the presence of the slot/scoop.

Properties of the theoretical inviscid flow field for the design Mach number of 2.5 are shown in figures 2 and 3. The variations of cowl and centerbody surface Mach number as well as the computational flow field mesh (from the method-of-characteristics analysis) are shown in figure 2. Figure 3 indicates the theoretical

static pressure variations for each surface. A quasi-one-dimensional analysis was used to design the subsonic diffuser contours. The static pressure distributions in the subsonic diffuser region ($x/R > 2.8$) shown in figure 3 were obtained from this same type of analysis, along with the actual diffuser area variation.

The theoretical, inviscid, total pressure recovery at the geometric throat ($x/R = 2.78$) upstream of the inlet terminal shock was 0.982. The throat Mach number of 1.30 resulted in a theoretical normal shock recovery of 0.962. The inlet throat section ($2.78 < x/R < 3.2$) had an initial area diffusion of $1^{\circ}$ equivalent conical expansion and a length equal to 4 hydraulic radii. The subsonic diffuser length measured from the geometric throat was 1.5 inlet diameters. The equivalent conical expansion of the complete subsonic diffuser (from geometric throat to diffuser exit) was $10^{\circ}$. The area variation through the inlet is shown in figure 4. The coordinates of the cowl and centerbody surfaces are listed in table I.

The model was designed to provide for inclusion of single rows of vortex generators on both the cowl and centerbody surfaces to prevent boundary-layer separation. The generator location was at $x/R = 3.37$ for both surfaces. Two different sets of vortex generators were available for testing with this model. Data are presented for model performance with each set of generators as well as with no generators on either surface. Figure 5(a) gives the pertinent design information for both sets of generators. Figure 5(b) indicates the placement of the generators on both surfaces with respect to the inlet support struts. Reference 3 gives a more complete discussion of the performance of the generator configurations within the inlet. For a more complete discussion of the design of the inlet, the reader is referred to reference 4.

## Bleed System

Provision was incorporated in the inlet design for bleed airflow removal through both the cowl and centerbody surfaces in the throat region. As indicated previously, the isentropic compression fan from the cowl and the cowl-lip oblique shock were canceled at the centerbody surface with an initial sharp turn followed by a prescribed contour. A slot/scoop bleed entrance was positioned immediately downstream of the cancellation point for boundary-layer control purposes. The slot/scoop coordinates are shown in figure 6. Results from reference 2 indicated that placement of the bleed slot/scoop upstream of such a cancellation point resulted in less than

desirable boundary-layer control. In addition, the higher surface static pressures downstream of the cowl shock impingement would hopefully result in better bleed pumping characteristics and higher bleed pressure recoveries in the centerbody cavity.

The different centerbody-bleed entrance configurations tested are shown in figure 6. Both the ram-scoop and flush-slot designs had the capability of using either a sharp or blunt downstream lip and any of three leading-edge configurations. The ram scoops were designed to capture 3 percent of the duct flow (based on inviscid calculations). The bleed airflow was ducted back through the centerbody to the hollow centerbody support struts (fig. 7). Internal "butterfly type" valves in the struts, which could be remotely positioned, were used to control the bleed backpressure. The bleed airflow was then ducted overboard to the free stream. Figure 6 indicates that the inclusion of the ram-scoop entrance resulted in the geometric throat of the inlet moving upstream to the bleed lip. In units of x/R, the upstream movement was 0.10. A decrease in the available flow area near the geometric throat also occurred and is shown in figure 4.

Two regions of porous bleed were incorporated on the cowl surface (fig. 8). The forward cowl-bleed region was located opposite to the centerbody slot/scoop and extended from x/R = 2.556 to x/R = 2.770. It was composed of 25 rows of 0.3175-centimeter-diameter normal holes located on centerlines that were 0.410 centimeter apart. The rows were staggered in a $60^{\circ}$ pattern to prevent inducing any circumferential variations in boundary-layer properties. The aft cowl-bleed region extended from x/R = 2.797 (just downstream of the geometric throat) to x/R = 3.105. It was composed of 36 rows of 0.3175-centimeter-diameter normal holes located on centerlines that were 0.408 centimeter apart. The aft holes were also staggered in a $60^{\circ}$ pattern. Nominal surface porosity of both bleed regions was 40 percent.

Cowl-bleed flows were discharged overboard through slot exits located on the external cowl surface. Bleed exit areas could be changed from configuration to configuration but not remotely. Cowl exit areas were sized for 1.4, 2.7, and 5.5 percent of the cowl-lip area.

## Model Instrumentation

The diffuser exit, mass flow ratio was calculated by using a calibrated choked plug and an average of eight static pressures in the cold pipe located 5.78 cowl-lip radii ahead of the plug exit (fig. 1(b)). Cowl-bleed flow ratios for both the forward and aft locations were determined from three circumferentially positioned static and total pressure surveys at their respective exits and from the measured exit areas (fig. 8). The centerbody-bleed mass flow ratio was determined from the measured total pressures in the hollow support struts, the strut valve choked-exit areas, and an experimentally determined flow coefficient (fig. 7). The overboard-bypass mass flow ratio was determined from a calibrated choked-exit area and the assumption that the bypass total pressure was equal to the average local static pressure at the bypass entrance. An experimentally determined flow coefficient was also determined for the overboard-bypass flow.

Static pressure variations along each surface throughout the inlet were determined from static pressure taps located along the top centerline of both the cowl and centerbody. Locations of the static pressure taps are given in table II.

The inlet flow field was surveyed by total pressure rakes at the throat, throat exit, mid-diffuser, and diffuser exit positions (fig. 9(a)). The details of the various rakes are given in figure 9(b). The rakes were circumferentially indexed to avoid mutual interference effects. All data from the rake surveys are presented in the form of measured pressures; that is, for locally supersonic flow, the pressures represent the measured values behind a locally normal shock.

The details of the steady-state total and static pressure instrumentation at the diffuser exit are shown in figure 9(c). The overall, diffuser exit, total pressure recovery was determined from an average of 72 total pressure measurements (six area-weighted tubes per rake). Three of the rakes (1, 7, 10) had three additional total pressure probes to better define the boundary layers on the cowl and centerbody at the diffuser exit. The presence of the four centerbody support struts was accounted for when the area weighting of the 12 rakes was accomplished. Wall static pressure measurements were made by using the 20 wall static pressure taps shown in figure 9(c).

Figure 10 indicates the static pressure and bleed flow survey measurements made for each centerbody-bleed entrance configuration.

## DISCUSSION OF RESULTS

### Range Sensitivity Comparison

A primary consideration in evaluating any supersonic cruise inlet is the range sensitivity of that inlet. Any particular inlet can be evaluated against a chosen reference inlet as to the number of kilometers of range gained or lost. Range sensitivity accounts for the influence of important parameters such as inlet total pressure recovery, bleed mass flow amounts, bleed total pressure recovery, and cowl drag. Past mission-analysis studies have shown that a reduction in inlet total pressure recovery of 0.01 results in a range decrement of 59 kilometers (32 n mi) and that an increase in bleed drag coefficient of 0.01 results in a range decrement of 75 kilometers (41 n mi) (ref. 5). The bleed drag coefficient accounts for both bleed mass flow and bleed total pressure recovery levels. Calculation of the bleed drag coefficient assumes that the flow is choked at the exit plane and is discharged in an axial direction.

A range decrement comparison of the final four inlet bleed configurations tested (table III) is shown in figure 11. In this comparison the configuration with no cowl bleed (Accb) was used as the reference configuration. Henceforth, configuration Accb will be termed the no-cowl-bleed configuration. The effects of bleed flow, bleed total pressure recovery, and diffuser exit total pressure recovery levels were accounted for in the comparison. It was assumed that all configurations would have the same cowl drag, so no cowl drag penalties were allotted. The configurations were compared for a critical inlet operating point (terminal shock located at the geometric throat) with a diffuser exit corrected airflow of 65.8 kg/sec (145 lb/sec). As noted previously, the TF30-P-3 turbofan engine requires a corrected airflow of 65.8 kg/sec for Mach 2.5 operation.

It can be seen from figure 11 that the cowl-bleed configurations experienced range decrements of from 48 kilometers (26 n mi) for configuration IIIAccb to 122 kilometers (66 n mi) for configuration IIAccb depending on the amount of bleed airflow removed. It is shown later (Cowl Bleed Development section) that addition of cowl bleed did result in higher diffuser exit pressure recoveries but that the increase in range afforded by this increased recovery was more than offset by the range decrement attributed to the increased cowl bleed. Thus, from range considerations alone, the no-cowl-bleed configuration would be the most desirable choice of those configurations tested. Of course, the final selection for an inlet bleed con-

figuration must also include consideration of other important performance criteria such as inlet stability margins and distortion levels. The final choice will often represent a compromise based upon the particular mission requirements.

## Centerbody Bleed Development

The inlet bleed development program reported herein was accomplished in two phases. Initially, various centerbody-bleed entrance configurations were tested and an optimum centerbody configuration chosen. This superior centerbody configuration was in turn used to determine the optimum cowl-bleed pattern and hence the optimum inlet bleed configuration. The various bleed configurations tested are described in table III. The first six configurations listed represent the centerbody-bleed configurations tested; the final five represent the cowl-bleed configurations tested. The designations for the various configurations are in agreement with those used in reference 4. Several points should be noted with regard to the centerbody-bleed configurations tested. As the table indicates, the cowl-bleed pattern was not fixed for this portion of the study, so caution must be exercised when comparing overall inlet performance levels. Also the vortex generators employed were not the same for all configurations tested. Finally, for this portion of the test program, the overboard-bypass system was sealed. It was not sealed for the cowl-bleed development portion.

A comparison of inlet total pressure recovery levels as a function of centerbody-bleed flow for inlet operation with the terminal shock at the geometric throat (critical) is presented in figure 12. For all configurations except VDccb and VIEccb, the following test procedure was employed: The centerbody-bleed exit area was set at the minimum opening for which the inlet terminal shock could be positioned at the geometric throat without unstart occurring. A control-room visual display was used to help position the terminal shock. This sequence was repeated with ever-increasing bleed exit areas (decreasing backpressures) to generate the curves shown. For configurations VDccb and VIEccb, the terminal shock was positioned at the geometric throat only for the smallest bleed exit area and was not repositioned for the other exit areas. For each configuration, the lefthandmost data point would correspond to the minimum centerbody bleed required to result in critical inlet operation. This operating point would have no subcritical stability margin. Any further

reduction in corrected airflow would result in immediate inlet unstart.

The curves indicate that configuration Accb could achieve a total pressure recovery of 0.898 for centerbody-bleed mass flows as low as 0.016 (which in this case was also the total bleed mass flow). All the other configurations exhibited approximately equal recovery levels, but in each case at least 0.02 centerbody-bleed mass flow was required. In particular, configuration VDccb achieved recoveries of 0.908, but a centerbody-bleed mass flow of at least 0.024 was required in addition to a cowl-bleed mass flow of 0.02.

Centerbody boundary-layer rake profiles for the configurations are shown in figure 13. The profiles indicate the quality of the centerbody boundary layer immediately downstream of the bleed entrance. Data are presented for minimum stable, critical, and representative supercritical operating conditions. For each configuration, the centerbody-bleed exit area was chosen so as to result in a bleed mass flow slightly greater than the respective minimum value shown in figure 12. No significant differences among the various profiles can be noted, so it appears that all centerbody-bleed entrance configurations provided acceptable boundary-layer control.

Centerbody-bleed performance for the various configurations is shown in figure 14. Configuration Accb achieved bleed recovery levels about equal to those of the other configurations but for smaller bleed flow amounts.

The centerbody-bleed-passage survey rake profiles shown in figure 15 indicate that differences did exist in the character of the flow entering the slot/scoop. Configurations Accb and C, which were blunt-lip configurations, had essentially flat profiles for all operating conditions. For the terminal shock downstream of the bleed entrance, locally supersonic flow existed over the entrance, and thus a bow shock existed ahead of the blunt lip. The flow entering the bleed passage was turned away from the bleed duct surface of the lip by the shock, and a "deadwater" region existed adjacent to this surface. Since the rake extended only partially across the passage, it indicated the deadwater (or base pressure) level. For minimum stable operation, the terminal shock was located in the bleed entrance, and again the bleed flow was turned away from the surface by the shock. The sharp-lip configurations (VDccb and VIEccb) exhibited flat profiles only for minimum stable conditions when the shock was in the bleed entrance. For configurations B and Fccb, static pressure distributions indicated that the terminal shock was located downstream of the en-

trance for minimum stable conditions. Since both configurations had sharp lips, the flow was not deflected away from the bleed duct surface as the profiles indicate. The somewhat different character of the profile of configuration Fccb was attributed to faulty total pressure measurements in the midchannel region.

The effects of slot and scoop bleed entrances on inlet steady-state performance are discussed in references 6 and 7. The inlet considered there was a two-dimensional, all-external-compression design with a flight Mach number of 2.0. The diffuser exit recovery for the inlet with a slot bleed entrance was found to be about 2 percentage points (0.02) higher than the recovery for the inlet with a ram-scoop bleed entrance (ref. 6). The authors attributed this recovery variation to a difference in the terminal shock structure near the bleed entrance. The recovery levels of figure 12 seem to reveal a similar trend. That is, the slot bleed configurations exhibited a slightly higher recovery on the average than did the ram-scoop bleed configurations. The study of reference 7 involved an investigation of the properties of the bleed flow entering a centerbody flush slot. It was determined that the bleed flow entered the slot as a concentrated jet flow near the downstream lip. The jet was directed away from the bleed duct surface, creating a deadwater region adjacent to this surface. These results agree qualitatively with those presented herein.

It is shown later (in the section Cowl Bleed Development) that the actual cowl-lip oblique shock impinged on the centerbody surface ahead of the theoretical location and was thus reflected toward the cowl surface. The static pressure rise across this oblique shock system appeared to restrict the centerbody-bleed recovery attained by the flush-slot configurations.

The data presented herein indicate that no appreciable differences in overall inlet operating characteristics existed for any of the configurations tested. Since configuration Accb exhibited equally high bleed total pressure recoveries for decreased bleed flows, the flush-slot, blunt-lip, dump-leading-edge, centerbody-bleed entrance configuration was chosen to be used in the cowl-bleed development portion of the study. It should also be noted that configuration Accb was able to maintain high inlet recovery levels for smaller amounts of centerbody-bleed flows than the other configurations.

## Cowl Bleed Development

As indicated previously, the cowl-bleed development was accomplished with the overboard bypass system operating. For each configuration, the choked-exit plug and overboard-bypass doors were adjusted so that the inlet was delivering the required corrected weight flow (65.8 kg/sec) with the terminal shock located at the geometric throat. This operating point is termed "critical." The amount of overboard bypass was as high as 0.06 (for configuration Accb). For all five configurations tested (table III), performance curves are presented. In addition, rake profiles and static pressure distributions for minimum stable, critical, and representative supercritical operating conditions are presented. As an aid to the reader, a certain consistency in figure symbols has been maintained. That is, the circular, square, and triangular symbols used to indicate, respectively, minimum stable, critical, and representative supercritical operating conditions have been used for both the rake profiles and the static pressure distributions for the respective operating conditions. For the diffuser exit rake profiles, only rake 1 profiles (fig. 9) are presented.

The performance levels for configuration Accb are shown in figure 16. With no cowl bleed, a diffuser exit recovery of 0.894 could be reached prior to unstart. Steady-state distortion levels varied from 10 to 13 percent for the terminal shock in the throat region. The centerbody-bleed exit area was adjusted to give a nominal 0.02 centerbody-bleed flow. This slight increase from the optimum bleed flow (0.016) provided some subcritical stability margin, as shown in figure 16.

The corresponding static pressure distributions and rake profiles for configuration Accb are presented in figure 17. The cowl-side static pressure distributions for critical and supercritical operating conditions (fig. 17(a)) indicate that an overpressure occurred at $x/R = 2.68$. As reference 4 points out, the theoretical analysis used to design the supersonic portion of the inlet was performed with the assumption that the cowl-lip was sharp and that thus the cowl shock was an attached shock. In reality, the cowl lip had a radius of 0.038 centimeter, and so the actual cowl shock was detached and stood 0.06 centimeter ahead of the leading edge. Since the analysis did not account for this standoff distance, the actual cowl shock impinged ahead of the desired centerbody location and was reflected, striking the cowl surface. The overpressure observed on the cowl surface was due to the reflected shock.

The cowl-side, boundary-layer rake profiles (fig. 17(c)) and the throat exit rake profiles (fig. 17(e)) indicate that the cowl-side boundary layer was apparently not in need of any bleed flow removal to remain attached. For Mach 2.5 operation, the inviscid cowl-surface Mach number diffused from 1.8 to 1.3 in the supersonic diffuser region. The cowl-side, boundary-layer rake profiles indicate that a normal shock total pressure recovery of 0.96 was achieved for the inviscid flow region, which is in agreement with the theoretically predicted level. The incompressible shape factor for the cowl-side boundary layer was computed for critical inlet operation and found to be 1.45. Since a shape factor of about 1.8 would indicate potential separation problems, the cowl-side boundary layer was not separated in the throat region. Thus, it appears that the original inlet design goal of shortening the supersonic diffuser to minimize the required cowl bleed was realized.

The mid-diffuser rake profiles of figure 17(f) indicate reduced total pressure recovery levels over those of the diffuser exit rake (fig. 17(g)). The mid-diffuser rake was located immediately downstream of the centerbody vortex generators. The reduced recovery levels are indicative of the presence of the trailing vortices and subsequent increased turbulent mixing. This feature was observed for all configurations tested.

Stability performance curves for configuration Accb are shown in figure 18. A concept for generating increased inlet stability is fully discussed in reference 8. The test reported therein indicated that large subcritical inlet stability margins could be provided if the bleed backpressure (bleed exit area) were varied so as to maintain a constant bleed total pressure recovery. For normal operation, the bleed exit area would be sized so as to provide for nominal bleed requirements. However, when the terminal shock would begin to move upstream in response to a flow disturbance, the bleed exit area would increase to allow increased bleed flow and to prevent inlet unstart. The test of reference 8 incorporated such a stability bleed system on the cowl surface. Conceptually, a similar system could be incorporated into the centerbody-bleed system.

Figure 18 presents centerbody-bleed performance curves for various bleed exit areas and the subsequent inlet operating levels. For these data, a given symbol represents a constant bleed exit area. The operating point corresponding to the lesser bleed flow and recovery represents critical operation; the other point (tailed symbol) represents the minimum stable operation. It should be noted that the use

of the symbols to present these data is not consistent with the use of the symbols to present the steady-state performance data corresponding to the optimum centerbody-bleed exit area. It can be seen that, from the normal operating point (circular symbol), the centerbody-bleed flow could be increased by about 0.019 if a constant bleed pressure recovery level were maintained ($P_{b1}/P_0 = 0.24$). In terms of allowable decrease in diffuser exit corrected airflow, a 4.1 percent reduction could be tolerated prior to unstart. This percentage reduction in corrected airflow for a constant bleed pressure recovery is termed "the constant pressure stability index." From the inlet performance curves, a diffuser exit recovery of 0.908 could be achieved prior to unstart. The stability data for configuration Accb were taken with slightly less overboard-bypass flow than was removed when the basic performance data were taken (fig. 16).

As table III indicates, configuration IIIAccb had a distributed forward-cowl bleed of constant porosity. All 25 rows of the forward-cowl-bleed region had a one-hole-open, five-holes-closed pattern; the aft cowl-bleed region was sealed. Figure 19 indicates the performance levels of this configuration. The minimum stable diffuser exit recovery was 0.896; the steady-state distortion varied from 10 to 13 percent for the terminal shock in the throat region.

Pressure distributions and rake profiles for the selected operating points are shown in figure 20. As expected, the cowl bleed did reduce the thickness of the cowl-side boundary layer, as shown by comparing figure 20(c) with figure 17(c) - the corresponding no-cowl-bleed profiles. An increased diffuser exit recovery near the cowl surface was also noted.

Figure 21 presents the stability performance for configuration IIIAccb. If a centerbody-bleed recovery of 0.24 were maintained in the bleed plenum, the centerbody-bleed flow could be increased by about 0.032 prior to unstart, with the resultant diffuser exit recovery of 0.939. The increase in total bleed mass flow was 0.042. The corresponding constant-pressure stability index was 9.2 percent.

Configuration IVAccb had only two rows of forward-cowl bleed, both of which were opposite to the slot opening on the centerbody. Two rows of aft-cowl bleed were also opened to provide for supercritical shock control. As indicated in figure 22, the minimum stable recovery was 0.900 for configuration IVAccb; the steady-state distortion varied from 10 to 14 percent for the terminal shock in the throat region. This configuration had no subcritical operating range. That is, the terminal

shock could not be positioned forward of the geometric throat without unstart occurring. Pressure distributions and rake profiles for the selected operating points are shown in figure 23.

Stability performance for configuration IVAccb is shown in figure 24. Maintaining a bleed plenum pressure recovery of 0.24 would allow a 0.034 increase in centerbody-bleed mass flow prior to unstart with a corresponding diffuser exit pressure recovery of 0.937. The increase in total bleed mass flow was 0.045. The resultant constant pressure stability index was 8.9 percent.

Configuration IAccb had a distributed foward-cowl-bleed pattern (one hole open, two holes closed) for the 13 bleed hole rows that spanned the slot opening on the centerbody. As with configuration IVAccb, two rows of aft-cowl bleed were completely open. The performance curves of figure 25 indicate that a minimum stable recovery of 0.898 was achieved; distortion levels were in the 10 to 13 percent range for the terminal shock in the throat region. In addition, only a small subcritical operating range existed. Pressure distributions and rake profiles are presented in figure 26. The increased forward-cowl-bleed capability of IAccb over that of IIIAccb resulted in a predictably thinner cowl-side boundary layer (figs. 23(c) and 26(c)). Also the increased cowl bleed allowed the terminal shock to be positioned further upstream prior to unstart (figs. 23(a) and 26(a)).

Stability performance is shown in figure 27 for configuration IAccb. If a centerbody-bleed recovery of 0.24 were maintained, a maximum increase in centerbody bleed of 0.029 could be achieved. The increase in total bleed mass flow was 0.042. The resultant diffuser exit pressure recovery would be 0.938 and the constant-pressure stability index about 9.1 percent.

Configuration IIAccb had the same cowl-bleed patterns as did IAccb. However, the forward-cowl-bleed exit area was increased so as to provide a supercritical bleed mass flow ratio of about 0.021. The aft-cowl-bleed exit area was unchanged.

Performance curves for this configuration are shown in figure 28. The minimum stable recovery achieved was 0.900. Distortion levels for the terminal shock in the throat region varied from 9 to 13 percent. A comparison of the distortion levels for configurations IAccb and IIAccb (figs. 25 and 28) indicates that the increased bleed capability did decrease the distortion level for the shock in the throat region; however, the minimum stable diffuser exit pressure recovery was essentially the same for the two configurations. Pressure distributions and rake profiles for configuration

HAccb are presented in figure 29.

Stability performance for configuration IIAccb is shown in figure 30. Maintaining a centerbody-bleed recovery of 0.23 would allow a 0.038 increase in centerbody-bleed flow prior to unstart. The increase in total bleed mass flow was 0.054. The resultant maximum diffuser exit pressure recovery would be 0.943, and the constant-pressure stability index would be 11.8 percent.

## Stability Performance Comparison

A comparison of the constant-pressure stability performance of the final five configurations tested is shown in table IV. The increase in total bleed mass flow removal through the centerbody and cowl regions between the normal operating point (optimum centerbody-bleed exit area) and the operating point prior to unstart (maximum centerbody-bleed exit area) was determined from the stability performance curves (figs. 18, 21, 24, 27, and 30). The table indicates that the stability performances of configurations IAccb, IIIAccb, and IVAccb were about equal, with constant-pressure stability indices of 9.1, 9.2, and 8.9 percent, respectively, being achieved. The corresponding increases in total bleed mass flow were 0.042, 0.042, and 0.045. Configuration Accb had a constant-pressure stability index of 4.1 percent with a total bleed mass flow increase of 0.019. For configuration IIAccb, the constant-pressure stability index was 11.8 percent, and the bleed mass flow increase was 0.054. The data indicate that each additional percentage point (0.01) of bleed mass flow removed beyond the no-cowl-bleed level of 0.034 resulted in an increase in constant-pressure stability index of from 2 to 5 percent.

The constant-pressure stability results achieved in this test verify that inlet tolerance to internal airflow disturbances can be significantly increased through the use of a so-called constant-bleed-pressure stability system in conjunction with the centerbody bleed. The implementation of this concept requires devices (so-called pressure relief valves) to vary the bleed exit area so as to achieve constant bleed plenum pressure. For the cowl stability bleed system (ref. 8), the exit area variation (or response) would have to be rapid since the available cowl-bleed plenum would be small. However, since the centerbody-bleed plenum would be much larger, the pressure relief valves need not have as rapid a response since many transients could be absorbed by the plenum.

The amount of inlet stability required will obviously be dependent on the particular mission. The steady-state inlet performance data presented indicate that the no-cowl-bleed configuration (Accb) was the superior configuration from a range degradation standpoint. If a larger amount of stability than the no-cowl-bleed configuration provided (4.1 percent) is required, the inlet designer is faced with several alternatives. If he is willing to accept the associated range degradation penalty, he can simply add a cowl performance bleed system to the basic centerbody-bleed system. The results presented herein indicate that stability indices as large as 12 percent could be expected, but range degradations of as much as 122 kilometer (66 n mi) must also be tolerated. Alternately, he could explore the possibility of adding a cowl-side stability system, either in addition to or in place of the centerbody stability system. Obviously, further testing would be required to determine stability levels and range degradations of such configurations.

## Steady-State Distortion Comparison

For all configurations reported herein, the overall diffuser exit recovery was about 0.90 for minimum stable operation. Up to the geometric throat station, the 4 percent loss (0.04) in total pressure in the inviscid core of the supersonic stream matched the theoretical predictions (figs. 17(c), 20(c), 23(c), 26(c), and 29(c)). However, the area-weighted recovery was somewhat less than 0.96 because of boundary-layer growth, being about 0.93 at the throat exit station for all configurations. Thus, an overall loss in recovery of 7 percent occurred up to the throat exit station, and the remaining 3 percent loss occurred in the subsonic diffuser downstream of the throat exit station. No attempt was made to determine where this loss occurred or what part of it was due to viscous effects. It is conceivable that a redesign of the subsonic diffuser, for example, a recontour of the diffuser surfaces and a redesign of the centerbody support struts, could reduce the total pressure losses.

An important characteristic of any inlet is the total pressure distortion (both steady state and dynamic) that it generates at the diffuser exit plane. The problem of inlet-engine distortion compatibility has been discussed in great detail in the literature. Certainly, it behooves the designer to minimize the distortion levels produced by the inlet. The steady-state data presented indicate that all configurations

had comparable levels of distortion, about 10 to 14 percent for the terminal shock located in the throat region.

A cause of the steady-state distortion levels encountered for the inlet tested is shown in figure 31. The figure presents the diffuser exit rake profiles for only one of the four flow quadrants. The profiles of rakes 2 and 12 indicate the cowl-side flow was in a state of incipient separation, but the profile of rake 1 indicates no such incipient separation. From figures 7 and 9, it can be seen that rakes 2 and 12 surveyed the flow immediately downstream of the bypass door openings. The results shown here are typical of all four flow quadrants and for all configurations tested. The bypass door entrance slots covered about the last one-third of the diffuser length and were in a region of rapid diffuser area variation (fig. 4). The entrance to the bypass doors provided an abrupt increase in diffuser area of about 10 percent. Each bypass door was a slotted plate that consisted of eight individual openings. Thus, the abrupt area change occurred eight times over the length of the bypass door. The apparent large-scale roughness in a region of rapid area variation could tend to separate the flow, at least locally, as indicated by a comparison of rakes 2 and 12 with rake 1. Although bypassing the flow has the effect of delaying separation, the surface roughness may have had a greater effect on the local flow.

The relative insensitivity of the inlet steady-state distortion levels with total bleed flow removal is shown in figure 32. Data are presented for each of the five inlet bleed configurations tested for three operating points: (1)minimum stable, (2)critical, and (3)representative supercritical ($P_2/P_0 = 0.87$). The data corresponding to critical inlet operation followed the expected trend of decreased distortion with increased bleed, but the data corresponding to minimum stable operation fail to indicate any such trend. As discussed previously, the distortion levels for this inlet appeared to be primarily due to the incipient flow separation from the cowl surface as induced by the overboard-bypass doors. Also data already presented have indicated that the inclusion of cowl bleed failed to appreciably increase the diffuser exit total pressure recovery performance. For either minimum stable or critical operation at the nominal centerbody bleed, less than a 0.01 increase in recovery was gained as a result of a removal of 0.03 cowl-bleed airflow (figs. 16, 19, 22, 25, and 28). The increase in recovery was not sufficient to offset the effect of the increased cowl bleed, and hence the cowl-bleed configurations experienced range degradation penalties. However, the increased cowl bleed was responsible

for the increase in inlet constant-pressure stability index (11.8 percent for IIAccb as compared to 5.8 percent for Accb). A further discussion of the distortion characteristics of this inlet design is given in reference 9.

## Angle-of-Attack Performance

The angle-of-attack performance for the five configurations tested is shown in figure 33. Data are presented for both the optimum and maximum centerbody-bleed exit areas. All data presented were taken with an operating bypass system. The following procedures were used to obtain the maximum angle-of-attack data for the optimum and maximum centerbody-bleed mass flows. For maximum angle of attack at critical inlet operation, (1) the inlet was set for critical operation (terminal shock at the geometric throat) for $0^{\circ}$ angle of attack, and (2) the model angle of attack was increased until unstart occurred. The inlet was restarted, and data were recorded for an angle of attack that was slightly less than the unstart angle. Determination of the maximum angle of attack for minimum stable inlet operation followed the same procedure as for critical inlet operation. For maximum angle of attack at supercritical inlet operation, (1) the inlet mass flow plug was fully retracted; (2) the model angle of attack was increased until unstart occurred; (3) the inlet was restarted and the model angle of attack was set at slightly less than the unstart angle; (4) the mass flow plug was then closed until the inlet unstarted; and (5) after the inlet was restarted, the plug was relocated near the position causing unstart. The data were then recorded. The same procedures were used to obtain the angle-of-attack data with maximum centerbody-bleed mass flow rates.

Configuration Accb had a maximum angle of attack of $2.55^{\circ}$ for the optimum bleed exit area; the corresponding critical angle of attack was $1.74^{\circ}$. Increasing the centerbody-bleed exit area to its maximum value resulted in a maximum angle of attack of $6.85^{\circ}$ and a critical angle of attack of $4.17^{\circ}$. As the curves indicate, the other configurations exhibited somewhat higher angle tolerances for the respective conditions. In particular for maximum centerbody bleed, configurations IIAccb and IIIAccb had maximum angles of attack that exceeded the wind tunnel strut limit of $8^{\circ}$.

## SUMMARY OF RESULTS

An inlet bleed development program was conducted in the Lewis 10- by 10-Foot Supersonic Wind Tunnel on a full-scale axisymmetric, mixed-compression inlet. The inlet was sized to provide the airflow requirements of the TF30-P-3 turbofan engine. At the design Mach number of 2.5, 55 percent of the supersonic area contraction occurred external to the cowl lip. Variations in the bleed entrance configurations on both the cowl and centerbody surfaces were investigated. The main results of this investigation are as follows:

1. The configuration with no cowl bleed exhibited the best range performance of all configurations tested. The configurations with cowl bleed suffered range decrements of from 48 to 122 (26 to 66 n mi) relative to the no-cowl-bleed configuration.

2. The no-cowl-bleed configuration achieved a minimum stable diffuser exit recovery of 0.894 with a centerbody-bleed mass flow ratio of 0.02. The cowl-bleed configurations had minimum stable recoveries as high as 0.900 for total bleed mass flow ratios as high as 0.055. The increased bleed mass flows were responsible for the range degradation penalties suffered by the cowl-bleed configurations.

3. Increasing the centerbody-bleed flow to a maximum amount allowed all configurations tested to achieve increased steady-state stability margins over the normal subcritical operating limits. If a constant centerbody-bleed plenum pressure were maintained, the data indicated that reductions in diffuser exit corrected airflow of from 4.1 percent for the no-cowl-bleed configuration to 11.8 percent for the maximum-cowl-bleed configuration could be tolerated prior to unstart.

4. Slightly higher diffuser exit recoveries were obtained when a flush-slot centerbody-bleed entrance was used rather than when a ram-scoop entrance was used.

5. With a centerbody-bleed flow of 0.02, the no-cowl-bleed configuration achieved a maximum angle of attack of $2.55^{\circ}$. With an increased centerbody-bleed flow, the configuration achieved a $6.85^{\circ}$ angle of attack prior to unstart. The vari-

ous cowl-bleed configurations achieved higher angles of attack for the respective operating conditions.

Lewis Research Center,
National Aeronautics and Space Administration,
Cleveland, Ohio, October 23, 1975,
505-04.

## REFERENCES


1. Anderson, Bernard H.: Design of Supersonic Inlets by a Computer Program Incorporating the Method of Characteristics. NASA TN D-4960, 1969.

2. Wasserbauer, Joseph F.; and Choby, David A.: Mach 2.5 Performance of a Bicone Inlet with Internal Focused Compression and 40-Percent Internal Contraction. NASA TM X-2294, 1971.

3. Neumann, Harvey E.; Wasserbauer, Joseph F.; and Shaw, Robert J.: Performance of Vortex Generators in a Mach 2.5, Low-Bleed, Full Scale 45-Percent-Internal-Contraction Axisymmetric Inlet. NASA TM X-3195, 1975.

4. Wasserbauer, Joseph F.; Shaw, Robert J.; and Neumann, Harvey E.: Design of a Very-Low-Bleed Mach 2.5 Mixed-Compression Inlet with 45 Percent Internal Contraction. NASA TM X-3135, 1975.

5. Bowditch, David N. ; et al.: Supersonic Cruise Inlets. Aircraft Propulsion, NASA SP-259, 1971, pp. 283-312.

6. Neale, M. C.; and Lamb, P. S.: Tests with a Two-Dimensional Intake Having All-External Compression and a Design Mach Number of 2.0. ARC-CP-937; ARC-25544, Aeronautical Research Council (NGTE-M-368), 1967.

7. Leynaert, J.: The Functioning of an Internal Boundary Layer Bleed on an External Compression Supersonic Air Intake. ONERA-TP-288, Office National d'Etudes et de Recherches Aerospatials, Paris (France), 1965.

8. Sanders, Bobby W.; and Mitchell, Glenn A.: Increasing the Stable Operating Range of a Mach 2.5 Inlet. AIAA Paper 70-686, June 1970.

9. Wasserbauer, Joseph F.; Neumann, Harvey E.; and Shaw, Robert J.: Distortion in a Full-Scale Bicone Inlet with Internal Focused Compression and 45 Percent Internal Contraction. NASA TM X-3133, 1974.

TABLE I. - INLET COORDINATES

(a) Cowl

| x R | r/R | x/R | r R |
|---|---|---|---|
| 2.0148 | 1.0000 | 4.0148 | 0.9745 |
| $2^{O}$ Internal | | 4.0683 | .9746 |
| cowl angle | | 4.1218 | .9748 |
| 2.2117 | 1.0069 | 4.1754 | .9749 |
| 2.2455 | 1.0079 | 4.2289 | .9751 |
| 2.2761 | 1.0084 | 4.2824 | .9753 |
| 2.3058 | 1.0086 | 4.3360 | .9756 |
| 2.3348 | 1.0086 | 4.3895 | .9759 |
| 2.3631 | 1.0082 | 4.4430 | .9761 |
| 2.3908 | 1.0075 | 4.4965 | .9763 |
| 2.4180 | 1.0065 | 4.5501 | .9765 |
| 2.4447 | 1.0053 | 4.6036 | .9768 |
| 2.4710 | 1.0038 | 4.6571 | .9770 |
| 2.4971 | 1.0021 | 4.7107 | .9771 |
| 2.5381 | 0.9993 | 4.7642 | .9774 |
| 2.5786 | .9967 | 4.8177 | .9776 |
| 2.6187 | .9944 | 4.8713 | .9779 |
| 2.6584 | .9924 | 4.9242 | .9781 |
| 2.6978 | .9906 | 4.9783 | .9783 |
| 2.7369 | .9889 | 5.0319 | .9785 |
| 2.7760 | .9872 | 5.0854 | .9787 |
| 2.7836 | .9869 | 5.1389 | .9790 |
| 2.8371 | .9850 | 5.1924 | .9792 |
| 2.8906 | .9831 | 5.2460 | .9794 |
| 2.9442 | .9813 | 5.2995 | .9796 |
| 2.9977 | .9794 | 5.3530 | .9798 |
| 3.0512 | .9778 | 5.4066 | .9800 |
| 3.1048 | .9763 | 5.4601 | .9802 |
| 3.1583 | .9754 | 5.5136 | .9805 |
| 3.2118 | .9748 | 5.5672 | .9807 |
| 3.2653 | .9745 | 5.6207 | .9808 |
| 3.3189 | .9743 | 5.6742 | .9809 |
| . | . | . | . |
| . | . | . | . |
| . | . | . | . |
| 3.9612 | .9743 | 5.8209 | .9809 |

(b) Centerbody

| x R | r R | x R | r R |
|---|---|---|---|
| 0 | 0 | 3.9612 | .6638 |
| $12.5^{O}$ Conical section | | 4.0148 | .6554 |
| 1.0001 | 0.2217 | 4.0683 | .6466 |
| $18.5^{O}$ Conical section | | 4.1218 | .6363 |
| 2.3749 | 0.6817 | 4.1754 | .6255 |
| 2.4408 | .7036 | 4.2289 | .6137 |
| 2.5068 | .7251 | 4.2824 | .6016 |
| 2.5733 | .7463 | 4.3360 | .5893 |
| 2.5831 | .7494 | 4.3895 | .5768 |
| Bleed slot | | 4.4430 | .5645 |
| 2.6883 | 0.7547 | 4.4965 | .5521 |
| 2.7283 | .7526 | 4.5501 | .5397 |
| 2.7836 | .7497 | 4.6036 | .5273 |
| 2.8371 | .7469 | 4.6571 | .5149 |
| 2.8906 | .7441 | 4.7107 | .5025 |
| 2.9442 | .7413 | 4.7642 | .4902 |
| 2.9977 | .7384 | 4.8177 | .4778 |
| 3.0512 | .7356 | 4.8713 | .4654 |
| 3.1048 | .7328 | 4.9248 | .4530 |
| 3.1583 | .7300 | 4.9783 | .4406 |
| 3.2118 | .7272 | 5.0319 | .4282 |
| 3.2653 | .7242 | 5.0854 | .4159 |
| 3.3189 | .7211 | 5.1389 | .4035 |
| 3.3724 | .7179 | 5.1924 | .3911 |
| 3.4259 | .7146 | 5.2460 | .3787 |
| 3.4795 | .7110 | 5.2995 | .3661 |
| 3.5330 | .7072 | 5.3530 | .3538 |
| 3.5865 | .7032 | 5.4066 | .3413 |
| 3.6401 | .6990 | 5.4601 | .3354 |
| 3.6936 | .6942 | . | . |
| 3.7471 | .6892 | . | . |
| 3.8007 | .6836 | . | . |
| 3.8542 | 0.6777 | 5.8209 | 0.3354 |
| 3.9077 | .6709 | | |

TABLE II. - STATIC-PRESSURE-TAP LOCATIONS

(a) Cowl

| x/R | |
|---|---|
| 2.088 | 3.158 |
| 2.195 | 3.212 |
| 2.302 | 3.319 |
| 2.409 | 3.426 |
| 2.462 | 3.533 |
| 2.516 | 3.640 |
| 2.569 | 3.747 |
| 2.623 | 3.854 |
| 2.677 | 3.961 |
| 2.730 | 4.175 |
| 2.784 | 4.389 |
| 2.837 | 4.604 |
| 2.891 | 4.818 |
| 2.944 | 5.139 |
| 2.998 | 5.468 |
| 3.051 | 5.607 |
| 3.105 | |

(b) Centerbody

| x/R | |
|---|---|
| 0.910 | 3.105 |
| .964 | 3.158 |
| 1.028 | 3.212 |
| 1.081 | 3.319 |
| 1.820 | 3.426 |
| 2.034 | 3.533 |
| 2.248 | 3.640 |
| 2.409 | 3.747 |
| 2.462 | 3.854 |
| 2.569 | 3.961 |
| 2.730 | 4.175 |
| 2.784 | 4.389 |
| 2.837 | 4.604 |
| 2.891 | 4.818 |
| 2.944 | 5.139 |
| 2.998 | 5.468 |
| 3.051 | 5.607 |

TABLE III. - DIFFUSER BLEED CONFIGURATIONS

| Configuration | Centerbody | Forward cowl (1 5 10 15 20 25) | Aft cowl (1 5 10 15 20 25 30 35) | Overboard bypass | Vortex generator configuration |
|---|---|---|---|---|---|
| VDccb[a] | Flush slot, sharp lip, dump leading edge | All 25 rows: one open, five closed | Rows 1 to 6: one open, three closed | No | I |
| VIEccb | Flush slot, sharp lip, modified leading edge | Rows 12 to 15: all open | Rows 1 to 6: one open, three closed | | I |
| Fccb | Flush slot, sharp lip, sloping leading edge | Sealed | Sealed | | I |
| Accb | Flush slot, blunt lip, dump leading edge | | | | II |
| B | Ram scoop, sharp lip, dump leading edge | | | | None |
| C | Ram scoop, blunt lip, dump leading edge | | | | None |
| Accb | Flush slot, blunt lip, dump leading edge | | | Yes | II |
| IIIAccb | | All 25 rows: one open, five closed | | | |
| IVAccb | | Rows 12 and 13: all open | Rows 5 to 17: all open | | |
| IAccb | | Rows 5 to 17: one open, two closed | Rows 5 to 17: all open | | |
| IIAccb[b] | | Rows 5 to 17: one open, two closed | Rows 5 to 17: all open | | |

[a] ccb denotes vortex generators on cowl and centerbody.

[b] Increased forward-cowl exit area.

TABLE IV. - STABILITY PERFORMANCE

| Configuration | Total bleed mass flow increase | Constant-pressure stability index, percent |
|---|---|---|
| Accb | 0.019 | 4.1 |
| IAccb | .042 | 9.1 |
| IIAccb | .054 | 11.8 |
| IIIAccb | .042 | 9.2 |
| IVAccb | .045 | 8.9 |

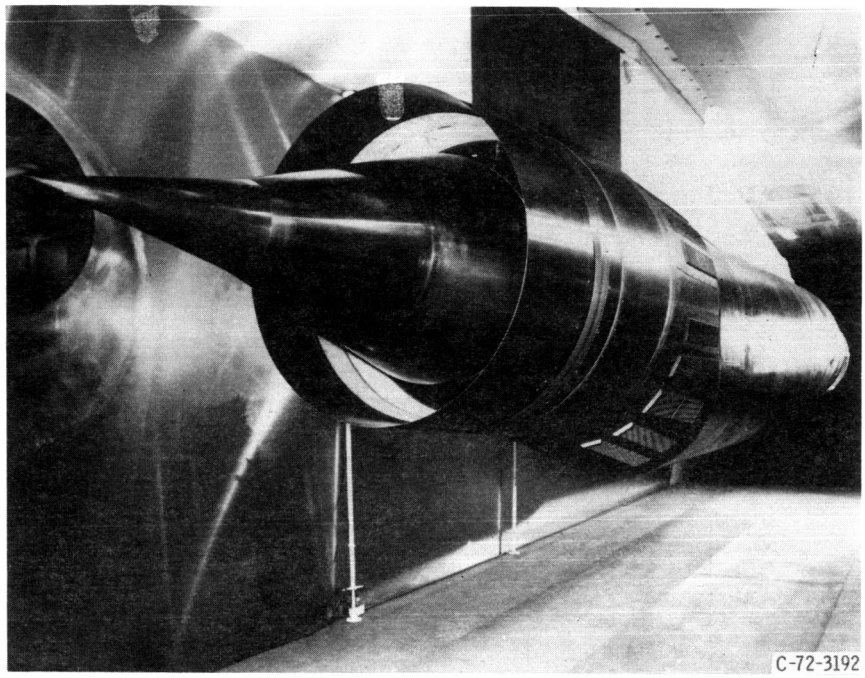


(a) Installation in 10- by 10-Foot Supersonic Wind Tunnel.

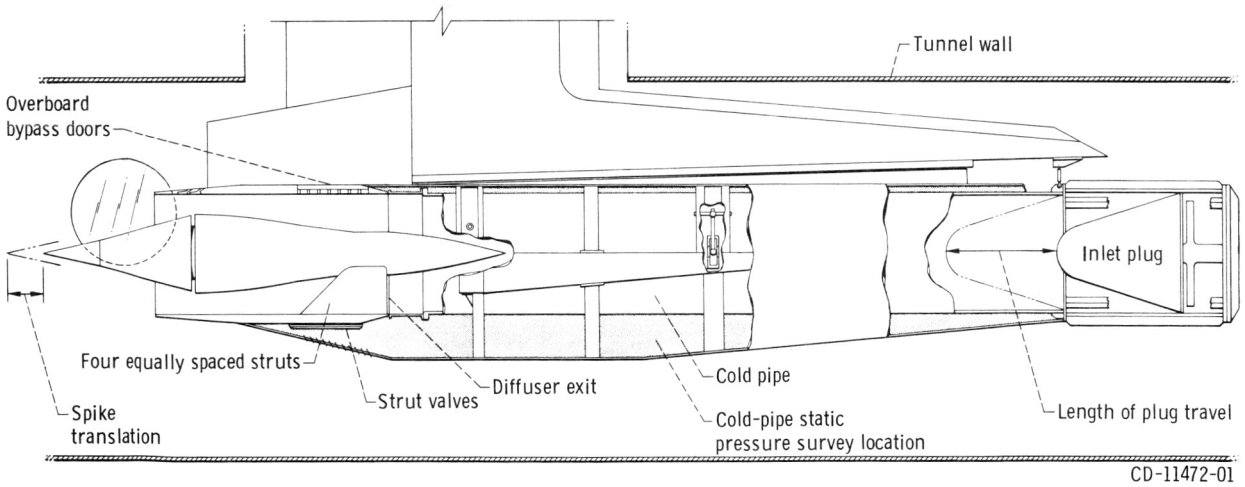


(b) Nacelle cutaway illustrating cold-pipe installation.

Figure 1. - Inlet model.

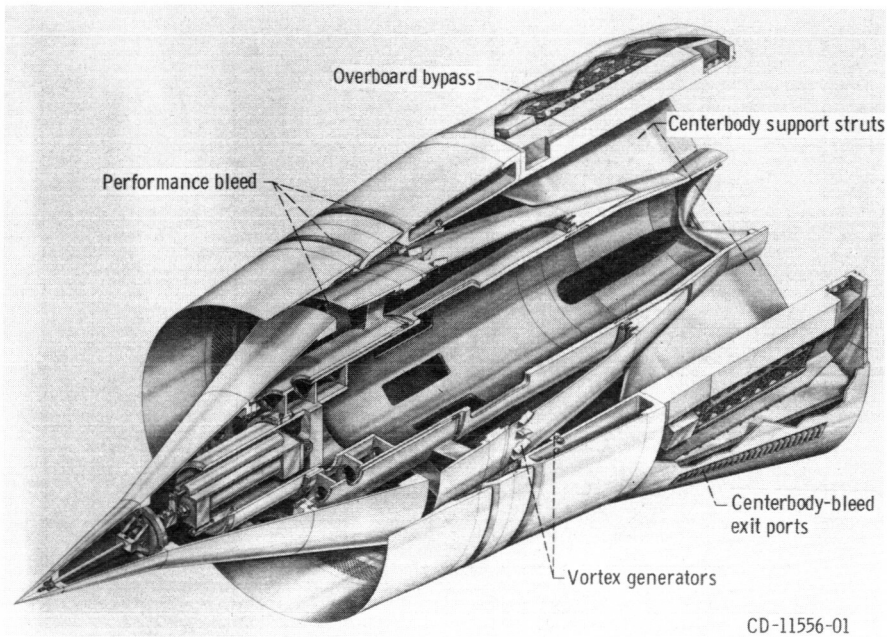


(c) Isometric view of model.

Figure 1. - Concluded.

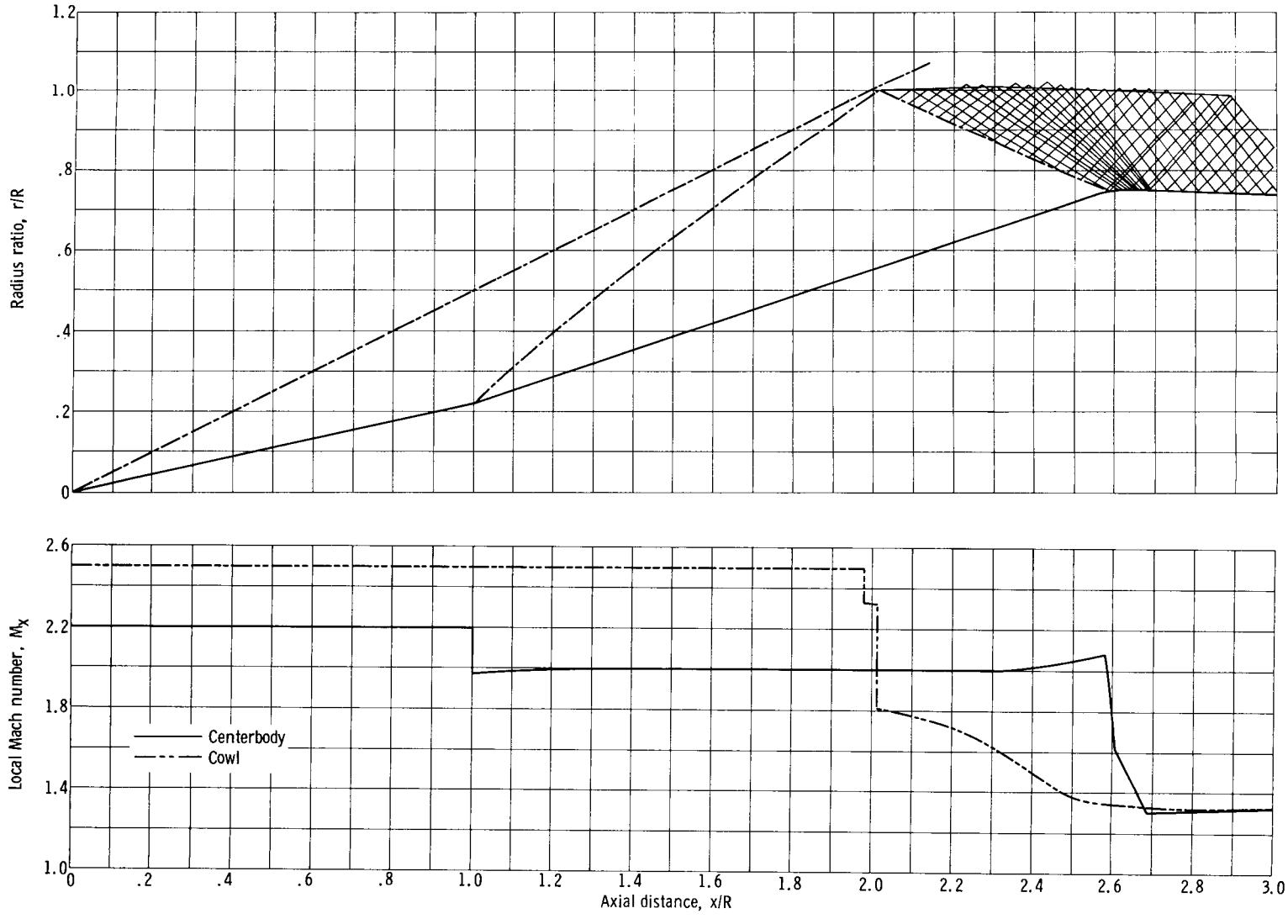


Figure 2. - Method-of-characteristics solution for design of Mach 2.5 inlet.

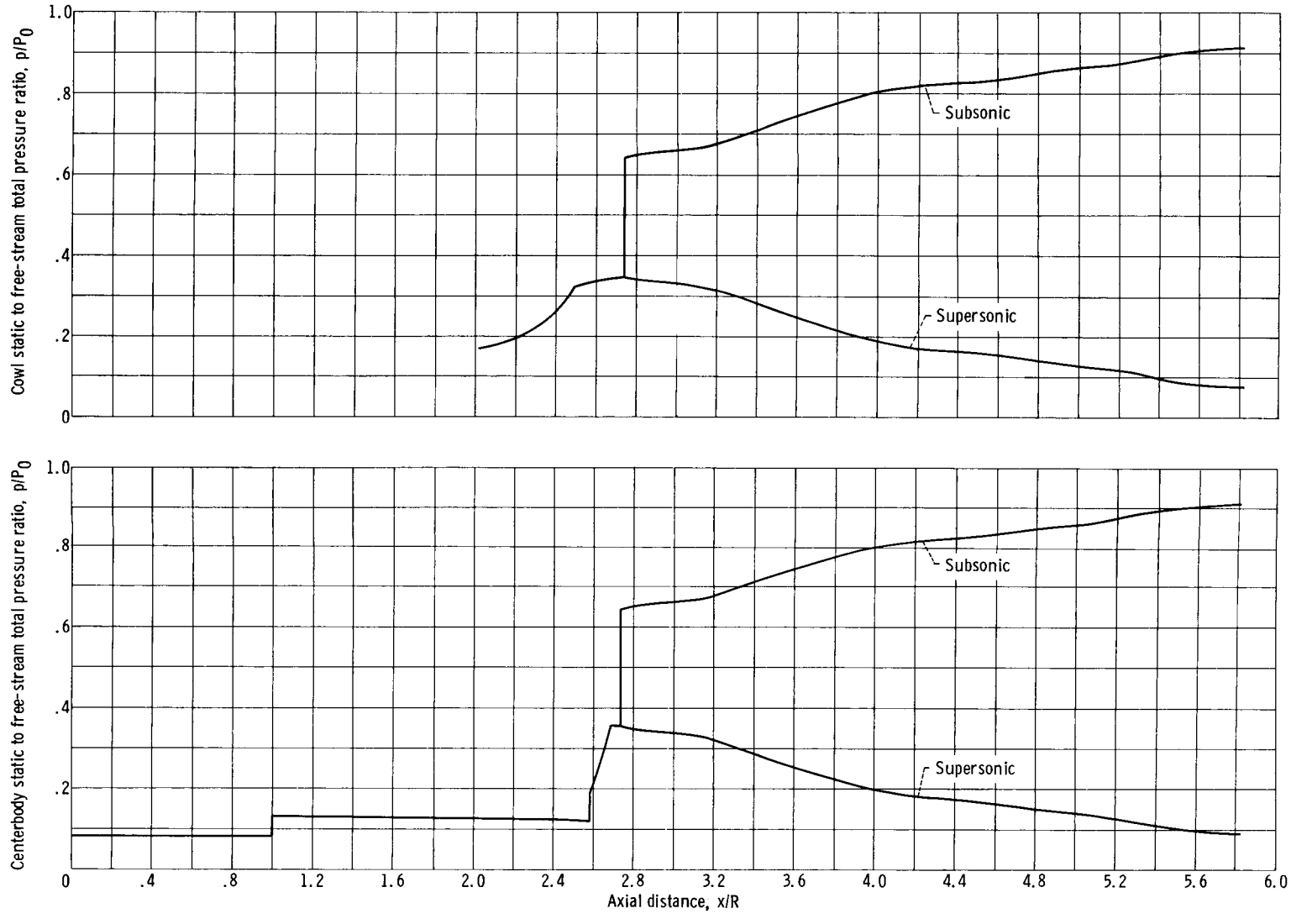


Figure 3. - Theoretical pressure ratios for Mach 2.5 inlet.

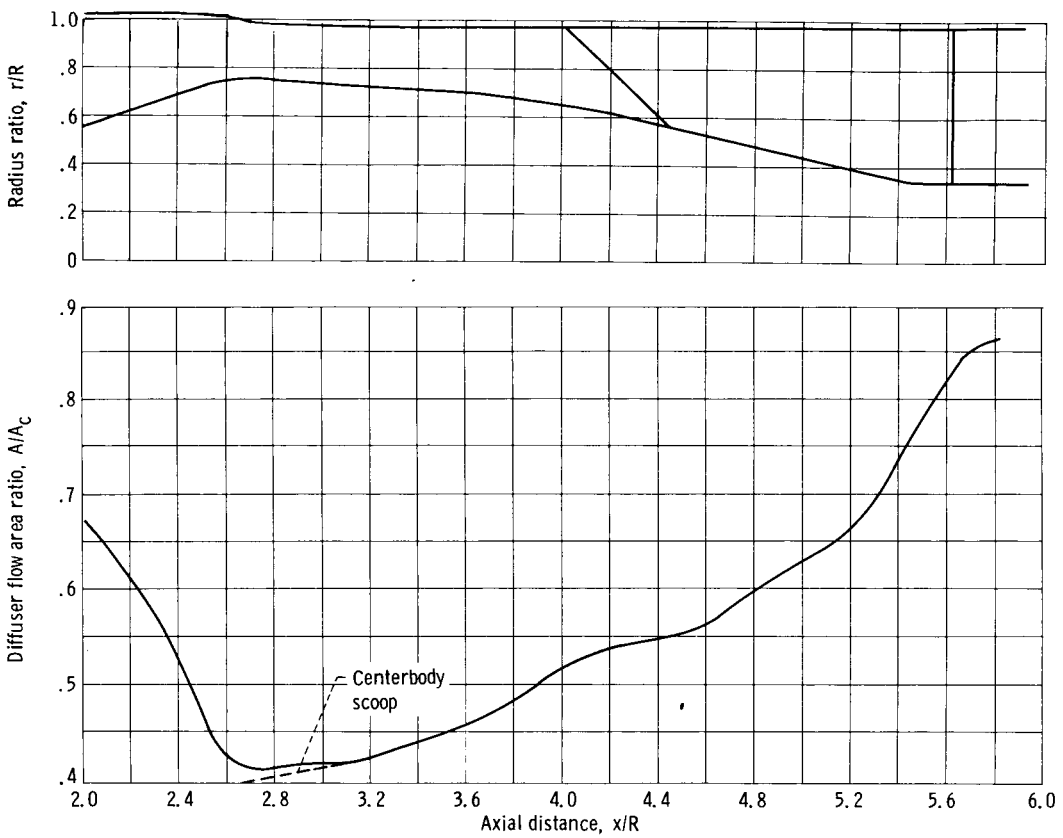


Figure 4. - Inlet area variation.

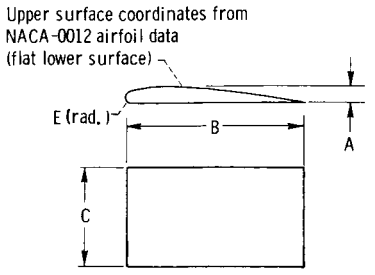


| Set | Location | Dimension, cm | | | | |
|---|---|---|---|---|---|---|
| | | A | B | C | D | E |
| I | Cowl | 0.305 | 5.044 | 2.54 | 9.682 | 0.051 |
| | Centerbody | .305 | 5.044 | 2.54 | 9.723 | .051 |
| II | Cowl | 0.229 | 3.048 | 1.52 | 4.841 | 0.030 |
| | Centerbody | .305 | 4.064 | 2.03 | 4.862 | .041 |

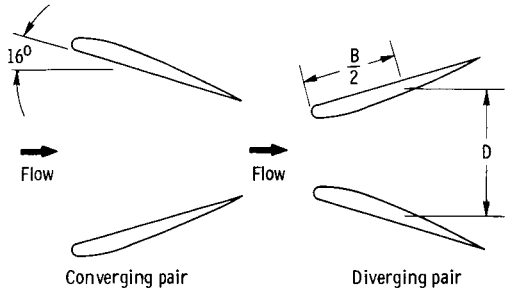


(a) Vortex generator design.

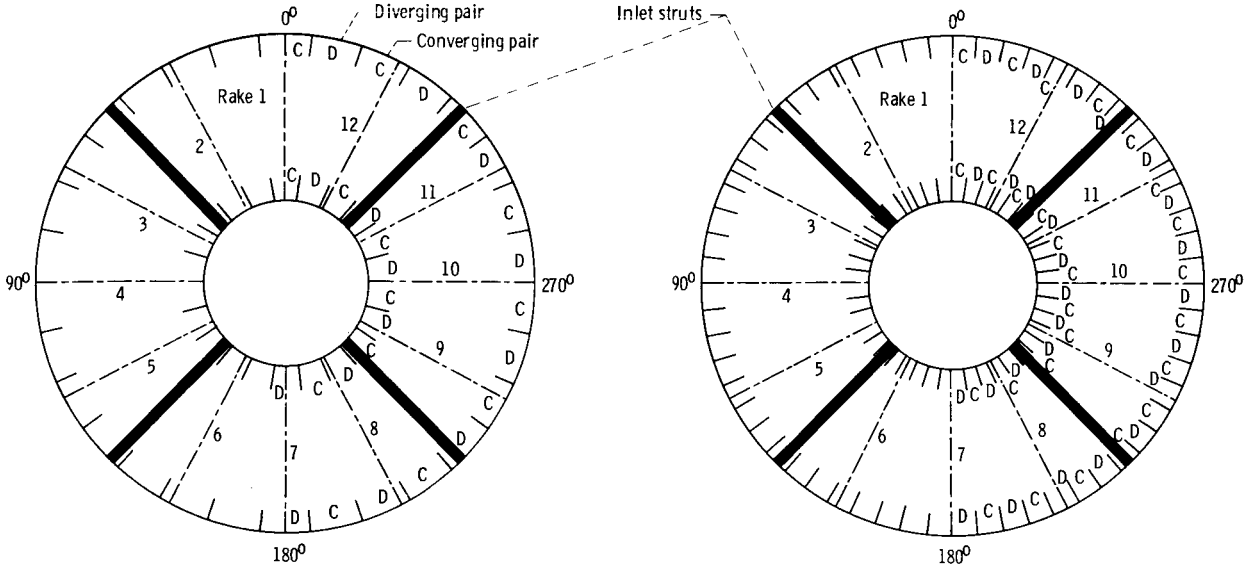


(b) Circumferential location, looking downstream.

Figure 5. - Vortex generator design and location.

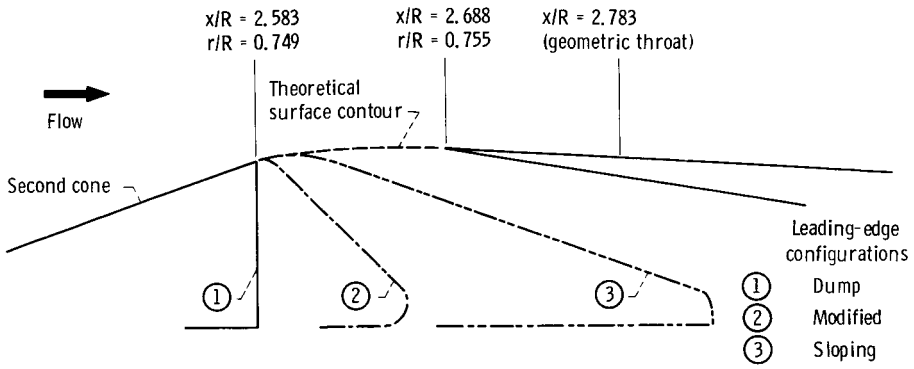


(a) Flush slot, sharp lip (configuration D).

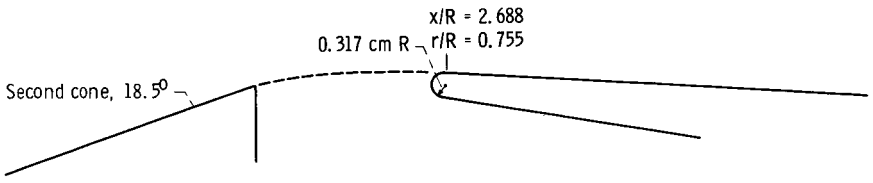


(b) Flush slot, blunt lip (configuration A).

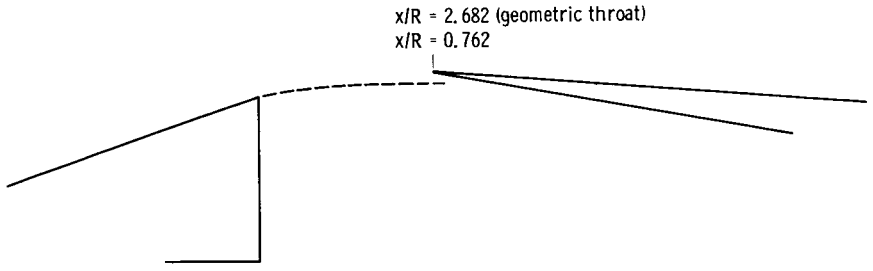


(c) Ram scoop, sharp lip (configuration B).

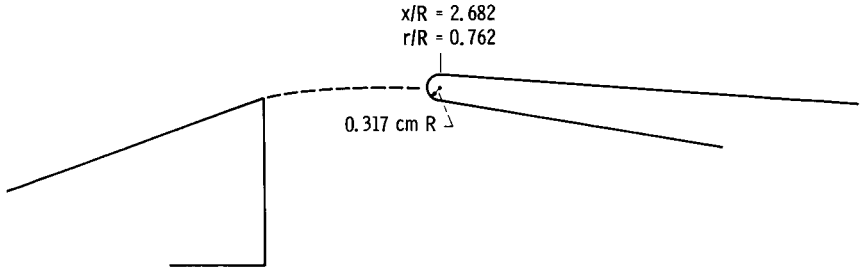


(d) Ram scoop, blunt lip (configuration C).

Figure 6. - Centerbody bleed configurations.

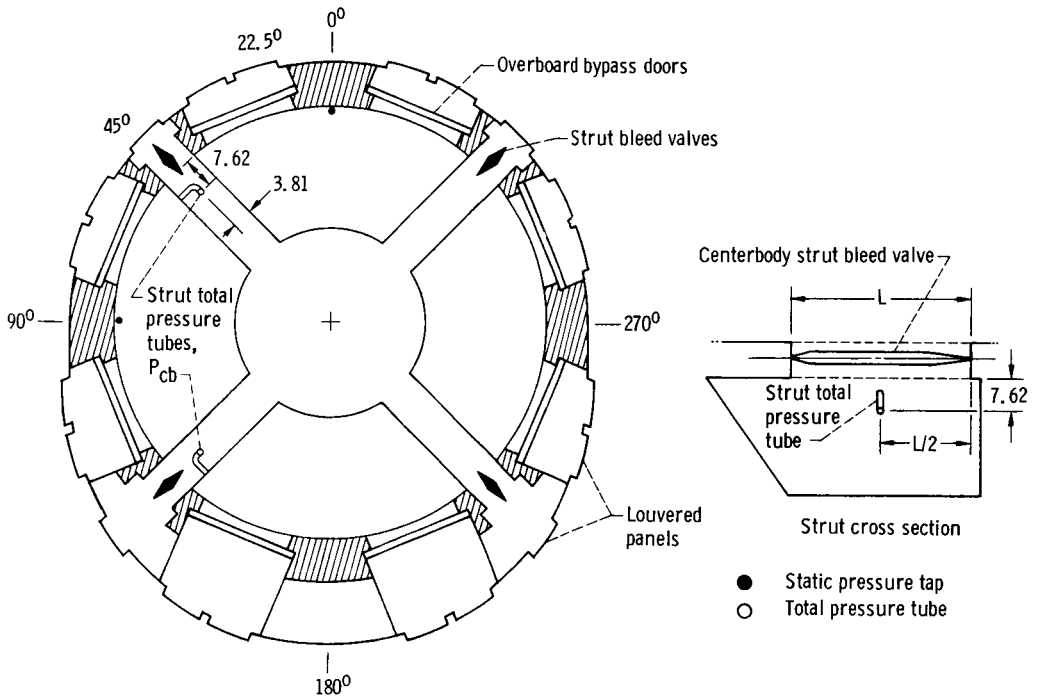


Figure 7. - Details of inlet support struts and strut valves. (All dimensions are in cm.)

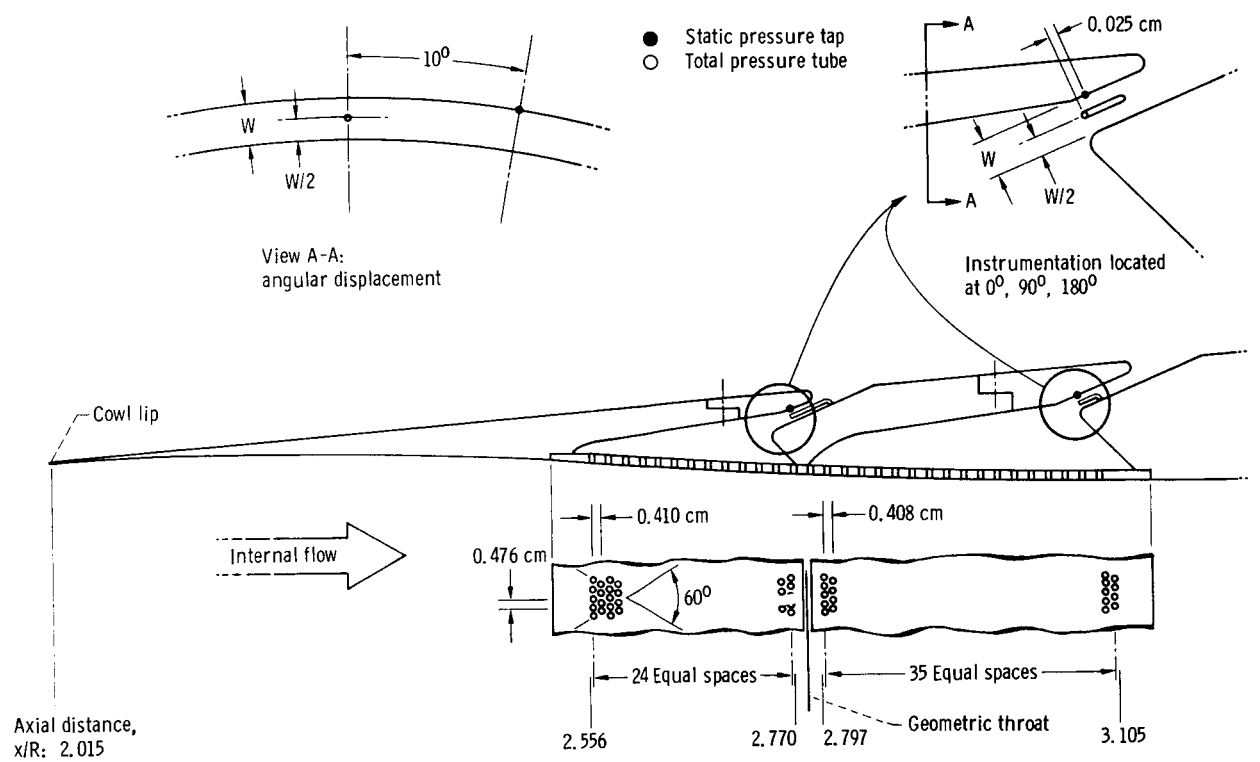


Figure 8. - Cowl-bleed detail. Diameter of bleed holes, 0.3175 cm.

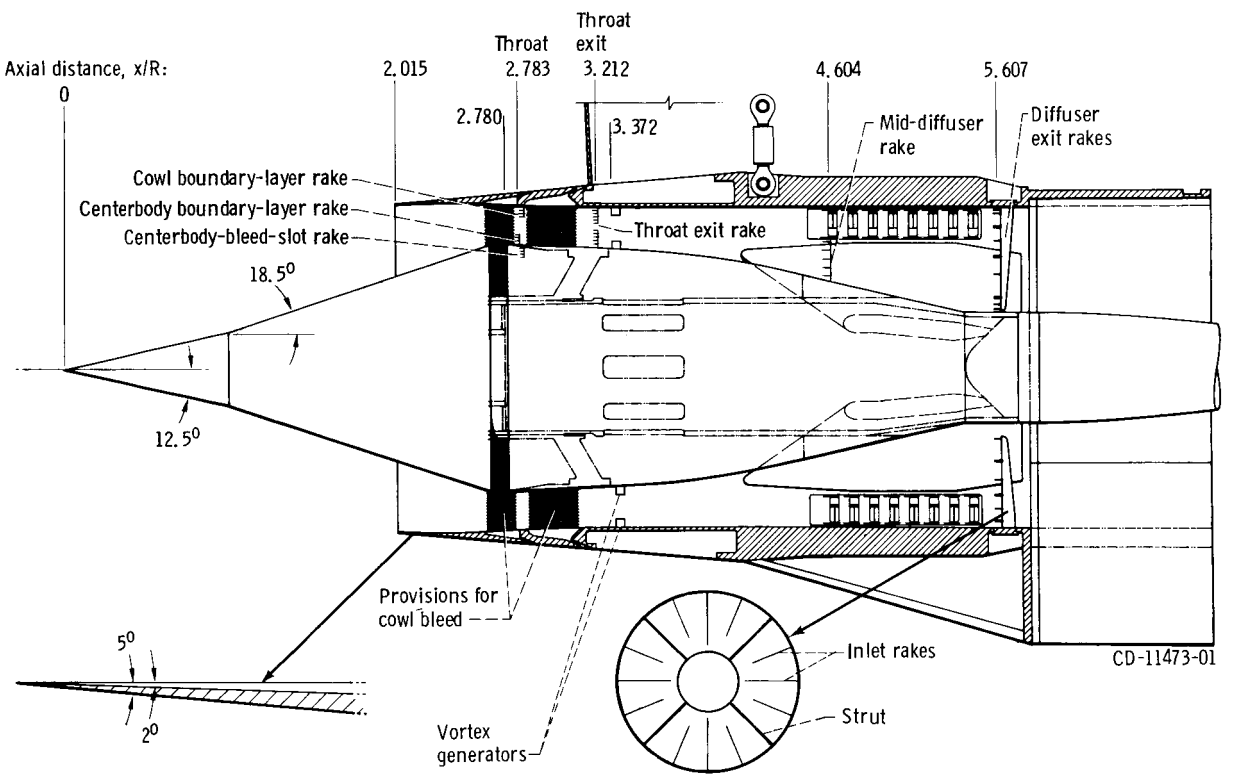


(a) Total pressure rake locations.

Figure 9. - Diffuser pressure instrumentation.

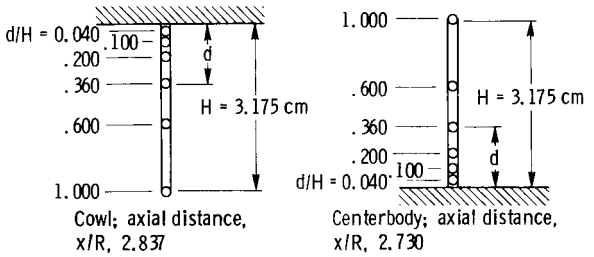


(b-1) Cowl and centerbody throat boundary-layer total pressure rakes. Circumferential position, $\varphi$, $10^0$.

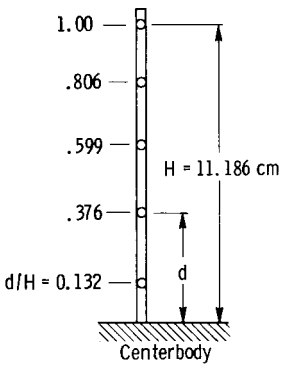


(b-2) Mid-diffuser total pressure rake. Circumferential position, $\varphi$, $0^0$; axial distance, x/R, 4.604.

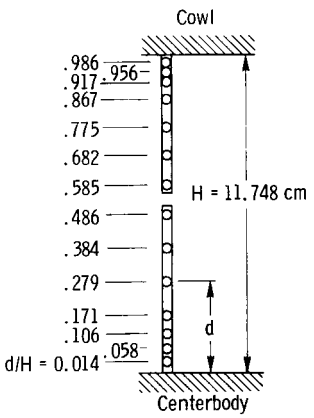


(b-3) Throat exit total pressure rake. Circumferential position, $\varphi$, $350^0$; axial distance, x/R, 3.212.

(b) Diffuser total pressure rakes.

Figure 9. - Continued.

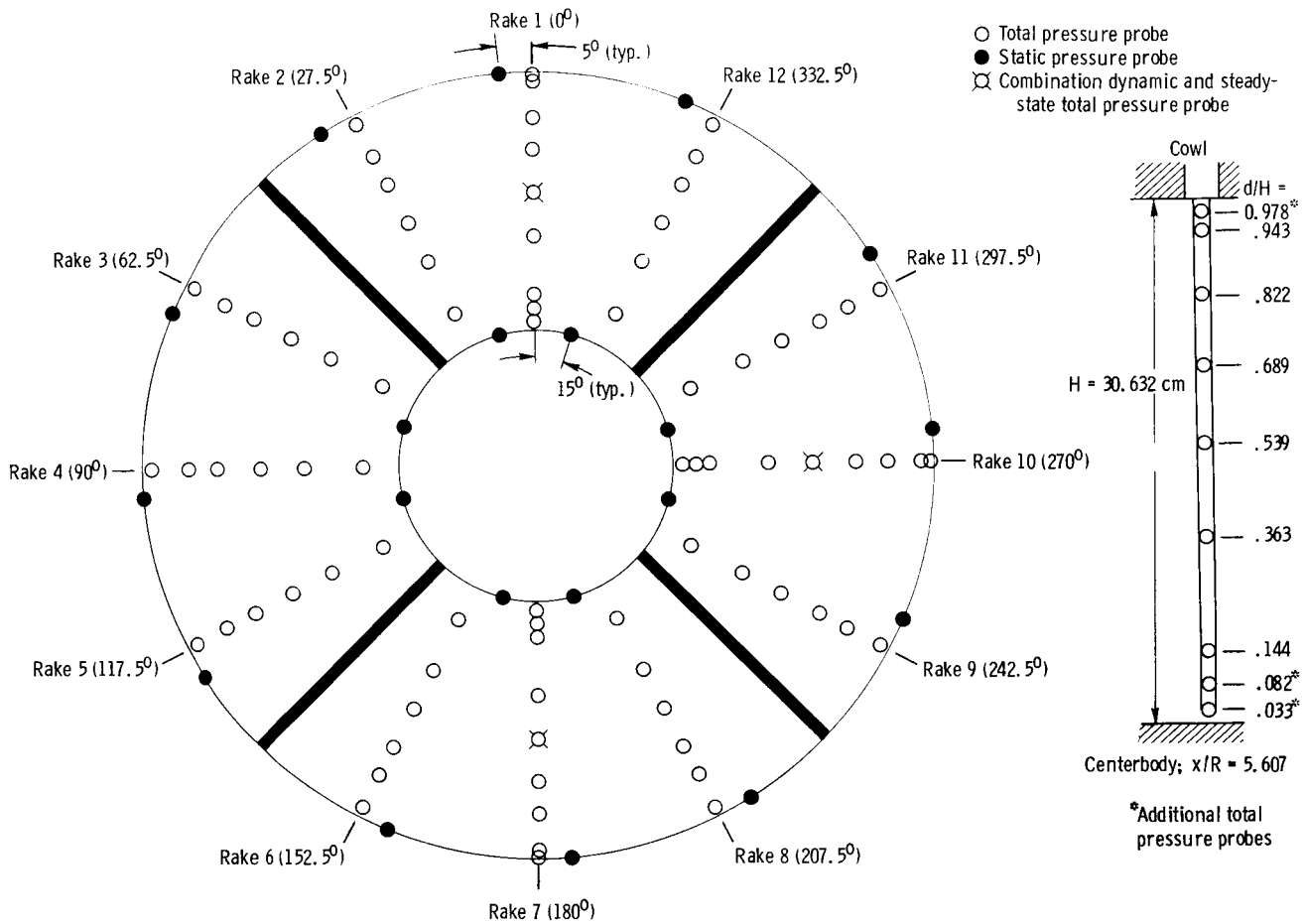


(c) Diffuser exit steady-state pressure instrumentation (looking downstream).

Figure 9. - Concluded.

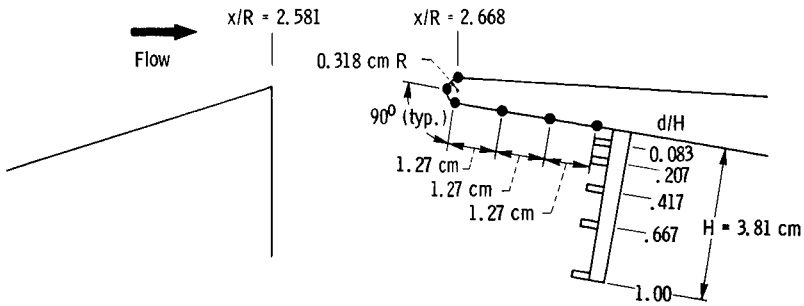


(a) Blunt-lip - flush-slot configuration.

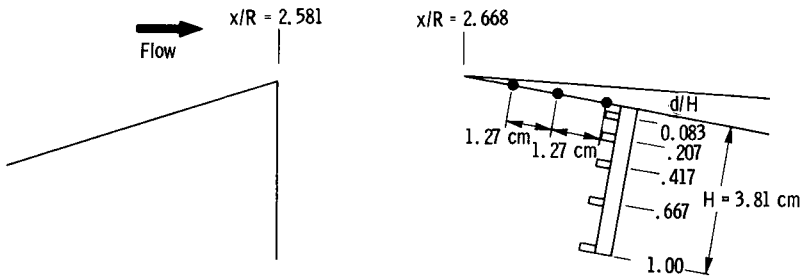


(b) Sharp-lip - flush-slot configuration.

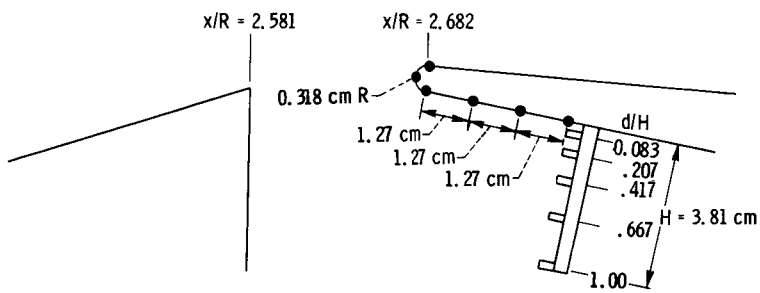


(c) Blunt-lip - ram-scoop configuration.

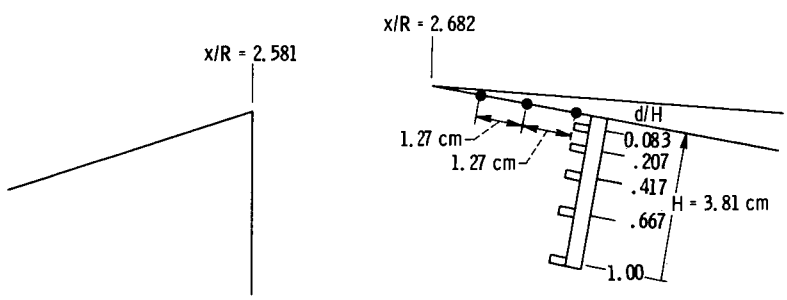


(d) Sharp-lip - ram-scoop configuration.

Figure 10. - Centerbody-bleed-slot instrumentation. Static-pressure-tap location, $0^{0}$; circumferential rake position, $\varphi$, $10^{0}$.

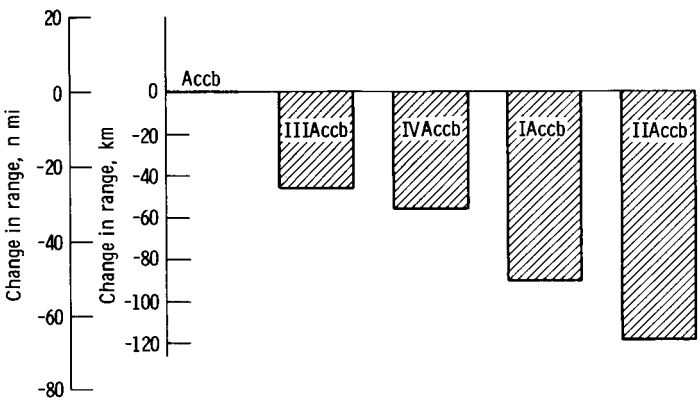


Figure 11. - Range decrements for configurations referenced to Accb.

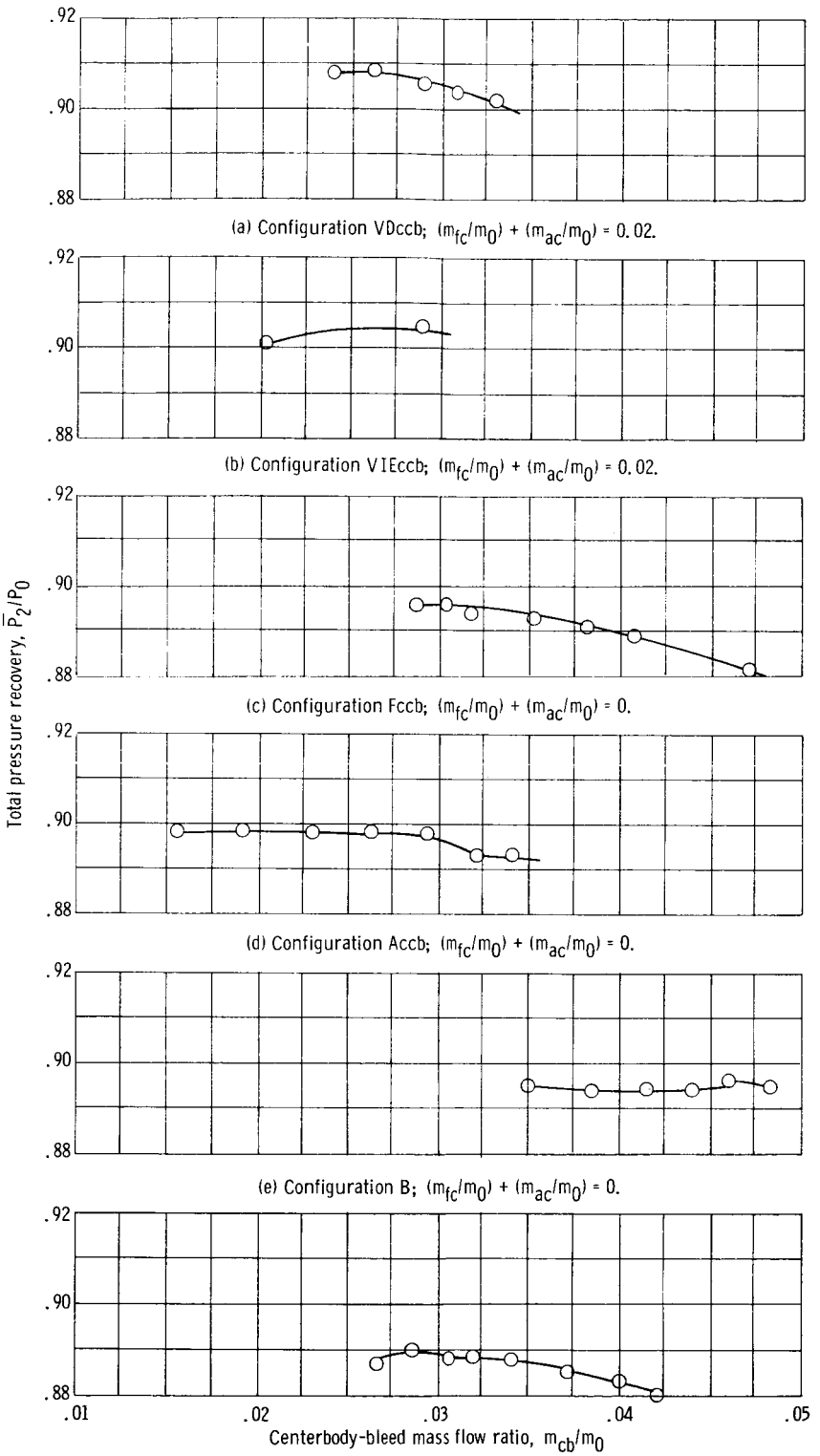


(a) Configuration VDccb; $(m_{fc}/m_0) + (m_{ac}/m_0) = 0.02$.

(b) Configuration VIEccb; $(m_{fc}/m_0) + (m_{ac}/m_0) = 0.02$.

(c) Configuration Fccb; $(m_{fc}/m_0) + (m_{ac}/m_0) = 0$.

(d) Configuration Accb; $(m_{fc}/m_0) + (m_{ac}/m_0) = 0$.

(e) Configuration B; $(m_{fc}/m_0) + (m_{ac}/m_0) = 0$.

(f) Configuration C; $(m_{fc}/m_0) + (m_{ac}/m_0) = 0$.

Figure 12. - Centerbody-bleed performance comparison.

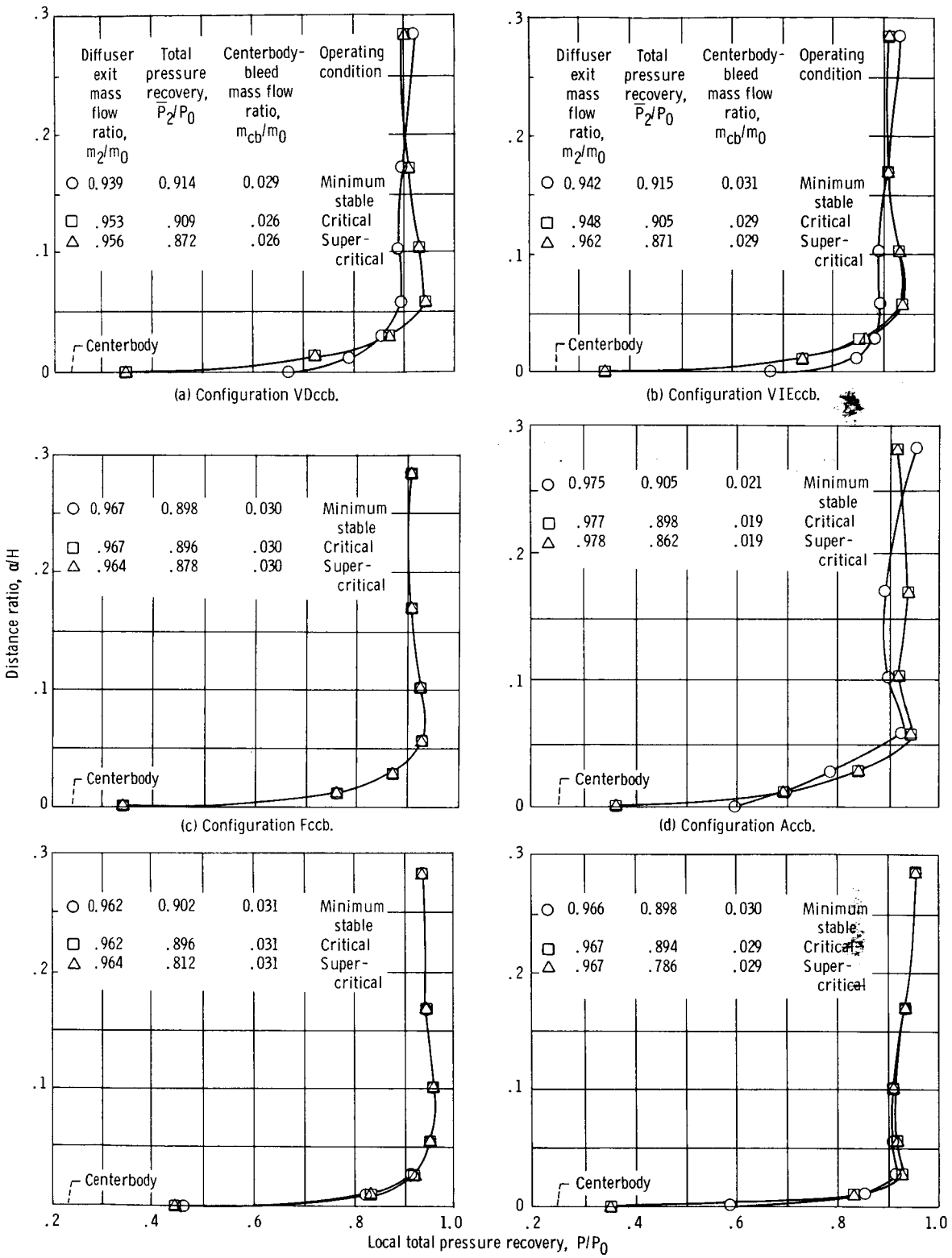


Figure 13. - Centerbody boundary-layer rake profiles. Free-stream Mach number, $M_0$, 2.5; angle of attack, $\alpha$, $0^o$; cowl-lip position parameter, $\theta_t$, $26.4^o$.

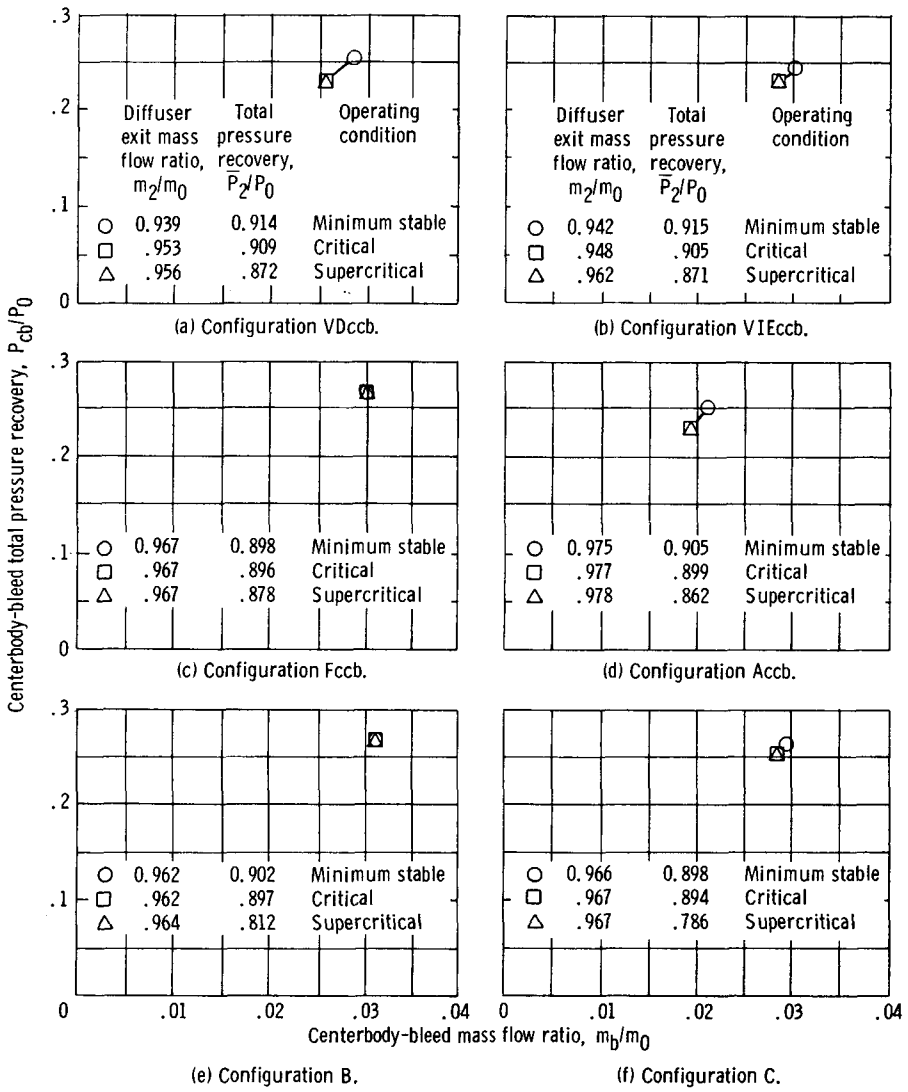


Figure 14. - Centerbody-bleed performance.

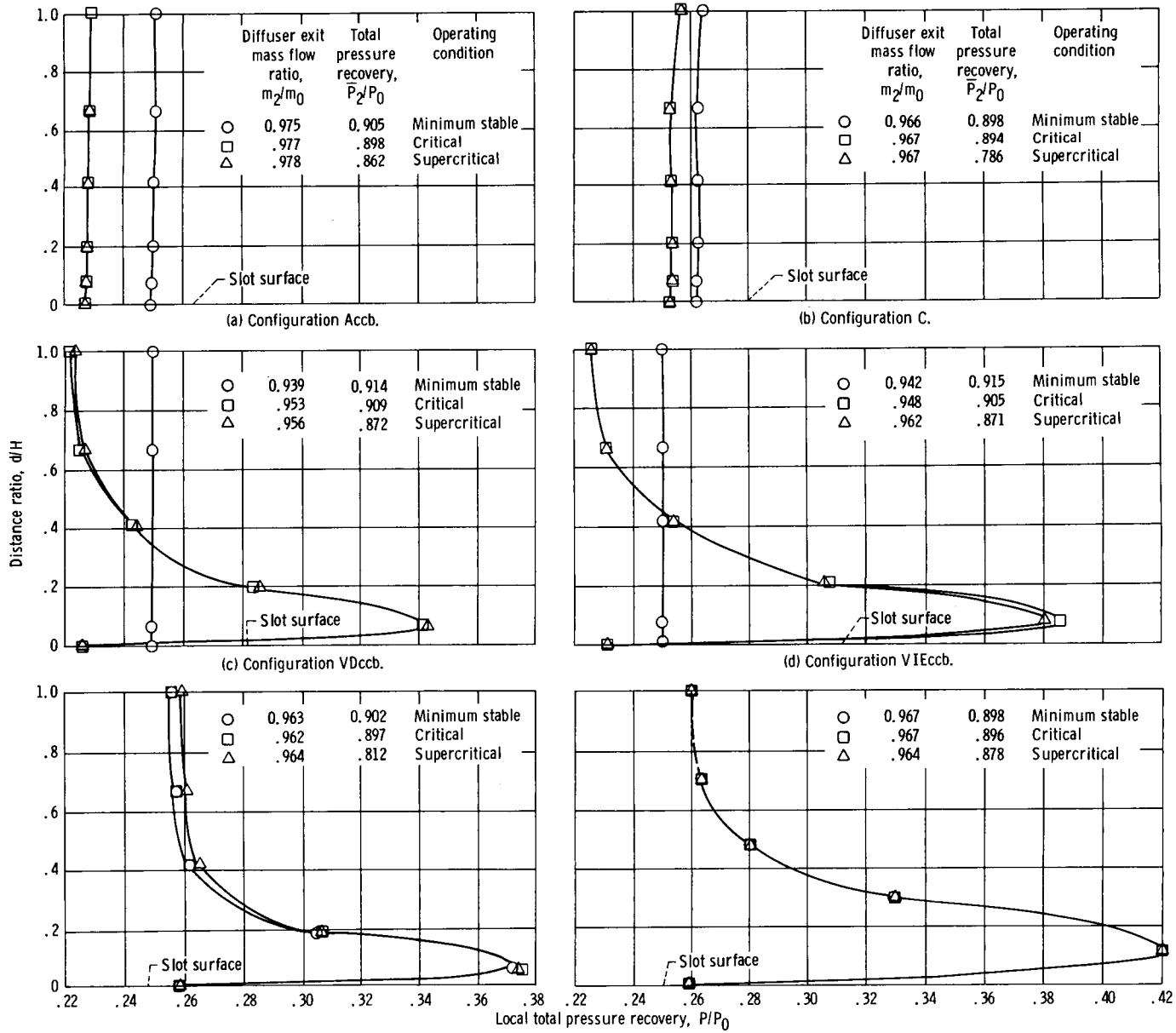


Figure 15. - Centerbody-bleed-passage survey rake profiles. (Rake height, H, 3.81 cm except for configuration Facb where H = 2.108 cm.)

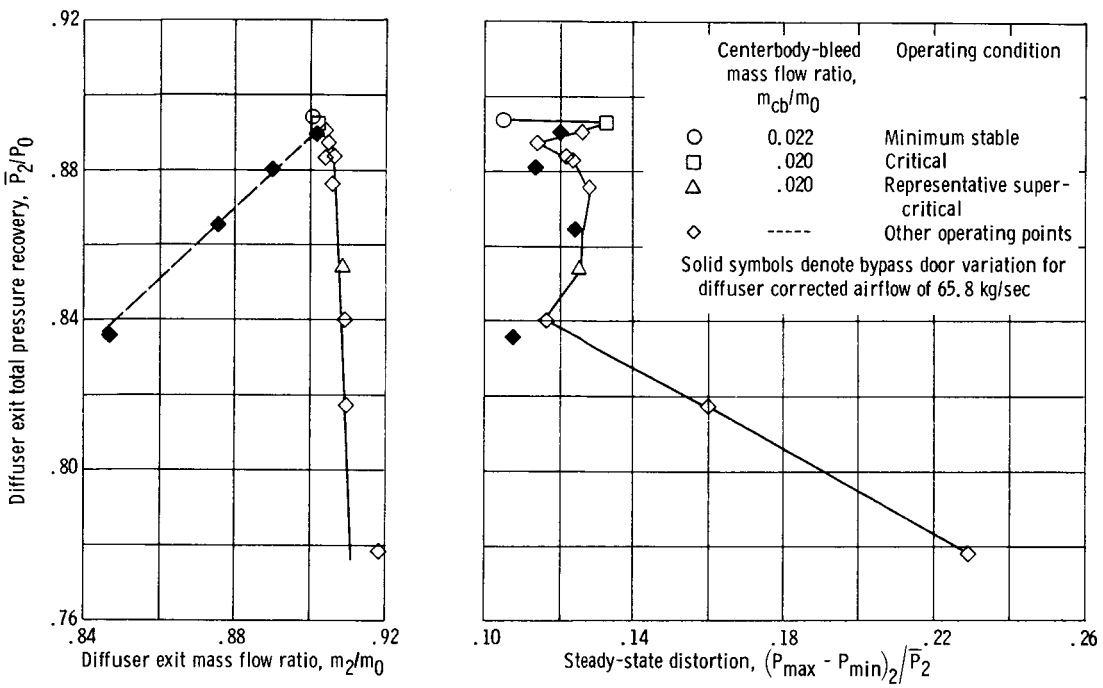


Figure 16. - Steady-state performance for configuration Accb. Free-stream Mach number, $M_0$, 2.5; angle of attack, $\alpha$, $0^o$; cowl-lip position parameter, $\theta_l$, $26.4^o$; bypass ratio, $m_{by}/m_0$, 0.06; forward-cowl-bleed mass flow ratio, $m_{fc}/m_0$, 0; aft-cowl-bleed mass flow ratio, $m_{ac}/m_0$, 0.

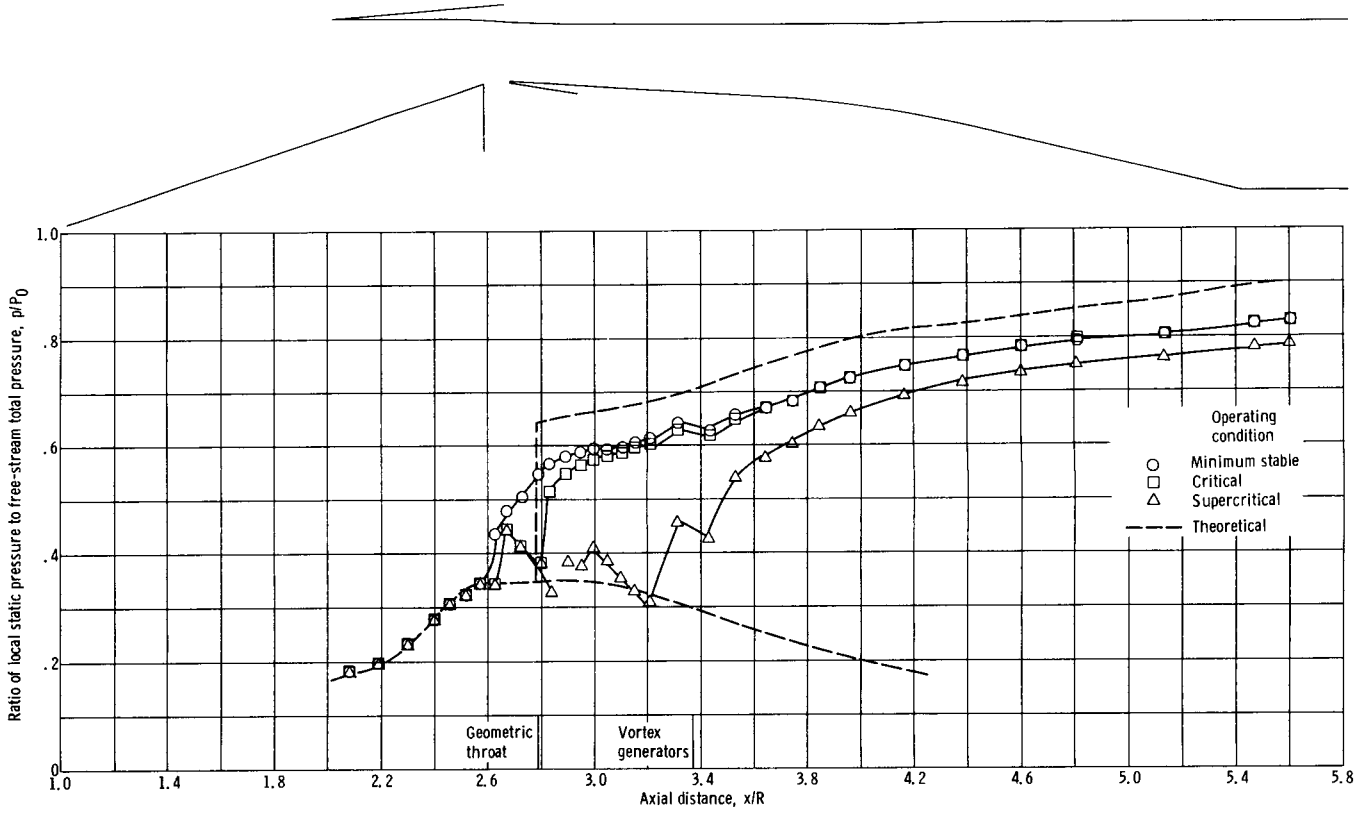


(a) Internal cowl-surface static pressure distributions.

Figure 17. - Diffuser performance for configuration Accb. Free-stream Mach number, $M_0$, 2.5; angle of attack, $\alpha$, $0^0$; cowl-lip position parameter, $\theta_t$, $26.4^0$; bypass mass flow ratio, $m_{by}/m_0$, 0.06.

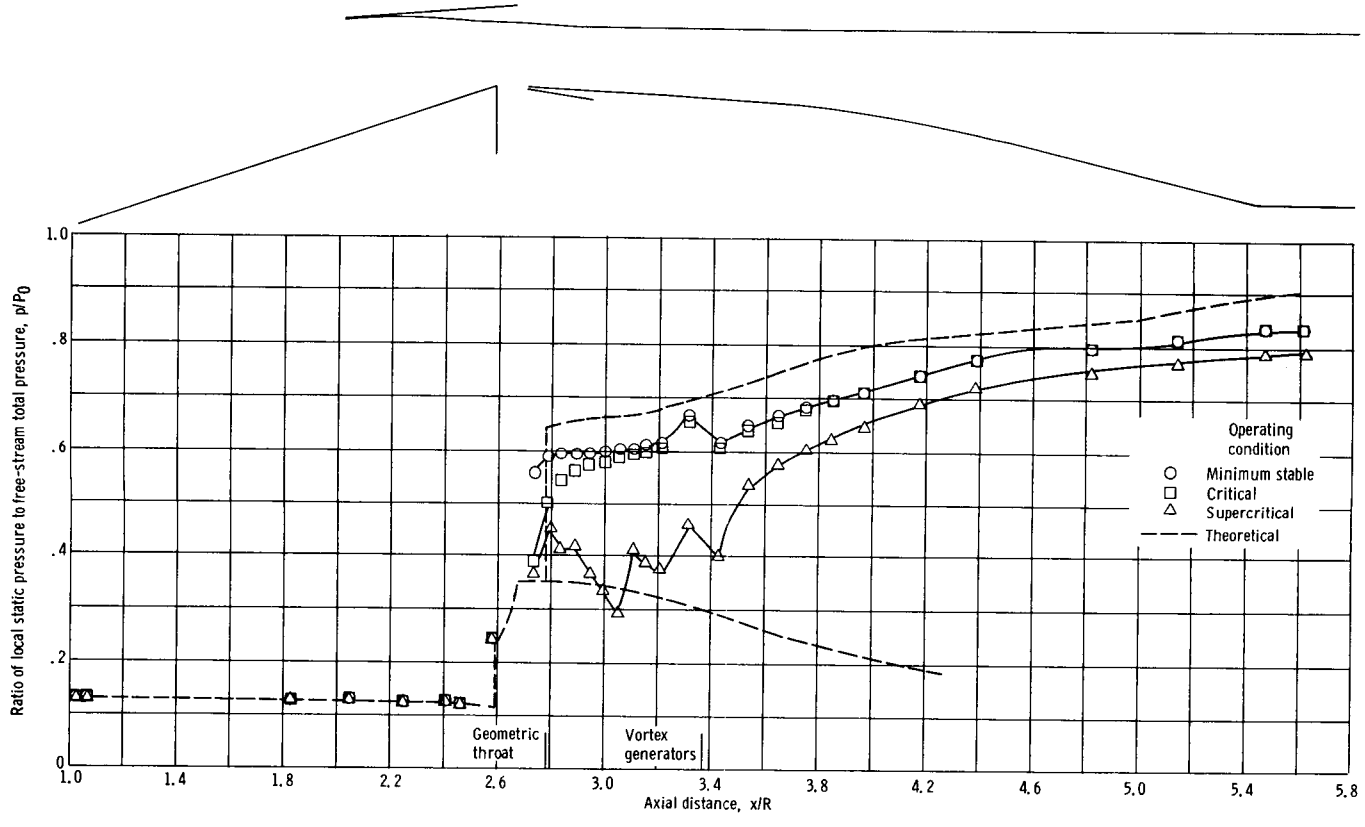


(b) Centerbody-surface static pressure distributions.

Figure 17. - Continued.

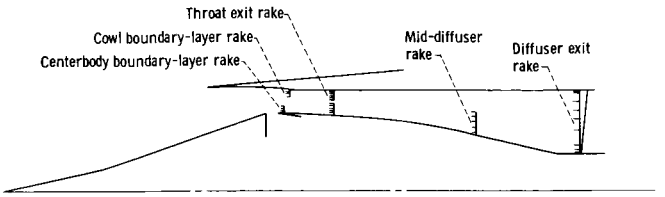


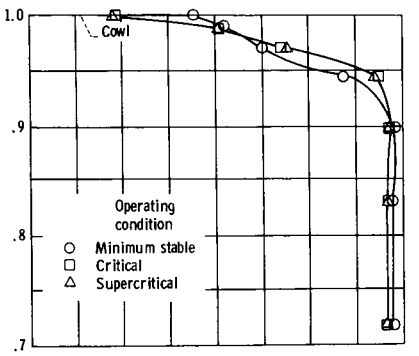


(c) Cowl boundary-layer rake profiles.

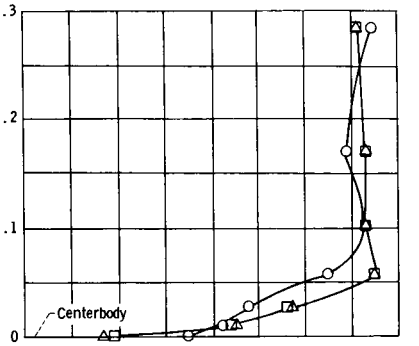


(d) Centerbody boundary-layer rake profiles.

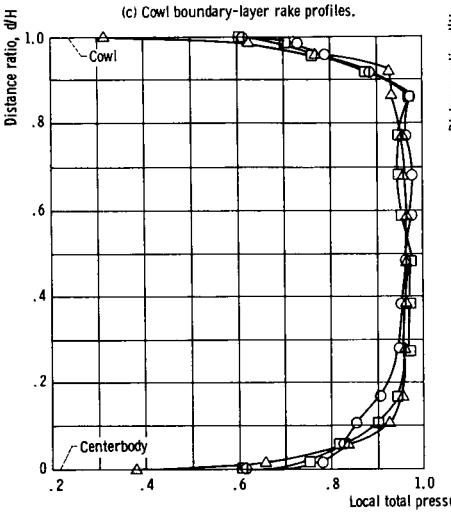


(e) Throat exit rake profiles.

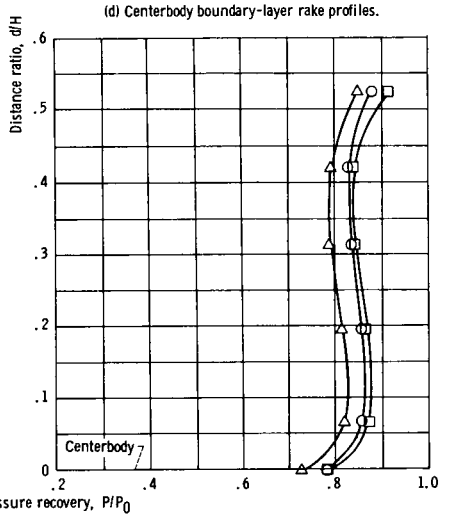


(f) Mid-diffuser rake profiles.

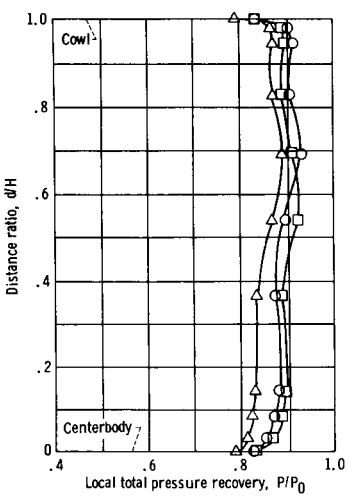


(g) Diffuser exit rake 1 profiles.

Figure 17. - Concluded.

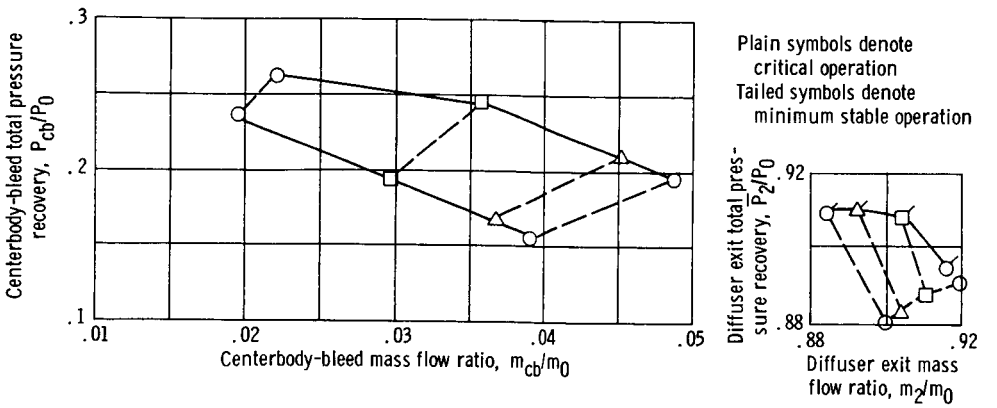


(a) Centerbody-bleed performance.

(b) Diffuser performance.

Figure 18. - Stability performance for configuration Accb. Free-stream Mach number, $M_0$, 2.5; angle of attack, $\alpha$, $0^0$; cowl-lip position parameter, $\theta_t$, $26.4^0$; bypass mass flow ratio, $m_{by}/m_0$, 0.06.

| | Centerbody-bleed mass flow ratio, $m_{cb}/m_0$ | Forward-cowl-bleed mass flow ratio, $m_{fc}/m_0$ | Operating condition |
|---|---|---|---|
| ○ | 0.020 | 0.015 | Minimum stable |
| □ | .019 | .013 | Critical |
| △ | .019 | .013 | Representative supercritical |
| ◇ | ----- | ----- | Other operating points |

Solid symbols denote bypass door variation for diffuser corrected airflow of 65.8 kg/sec

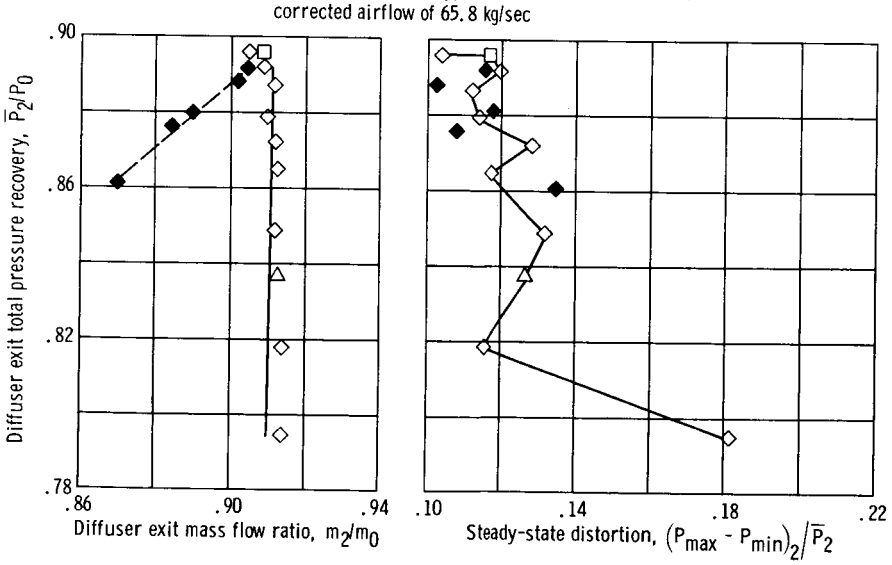


Figure 19. - Steady-state performance for configuration IIIAccb. Free-stream Mach number, $M_0$, 2.5; angle of attack, $\alpha$, $0^0$; cowl-lip position parameter, $\theta_t$, $26.4^0$; bypass mass flow ratio, $m_{by}/m_0$, 0.05; aft-cowl-bleed mass flow ratio, $m_{ac}/m_0$, 0.

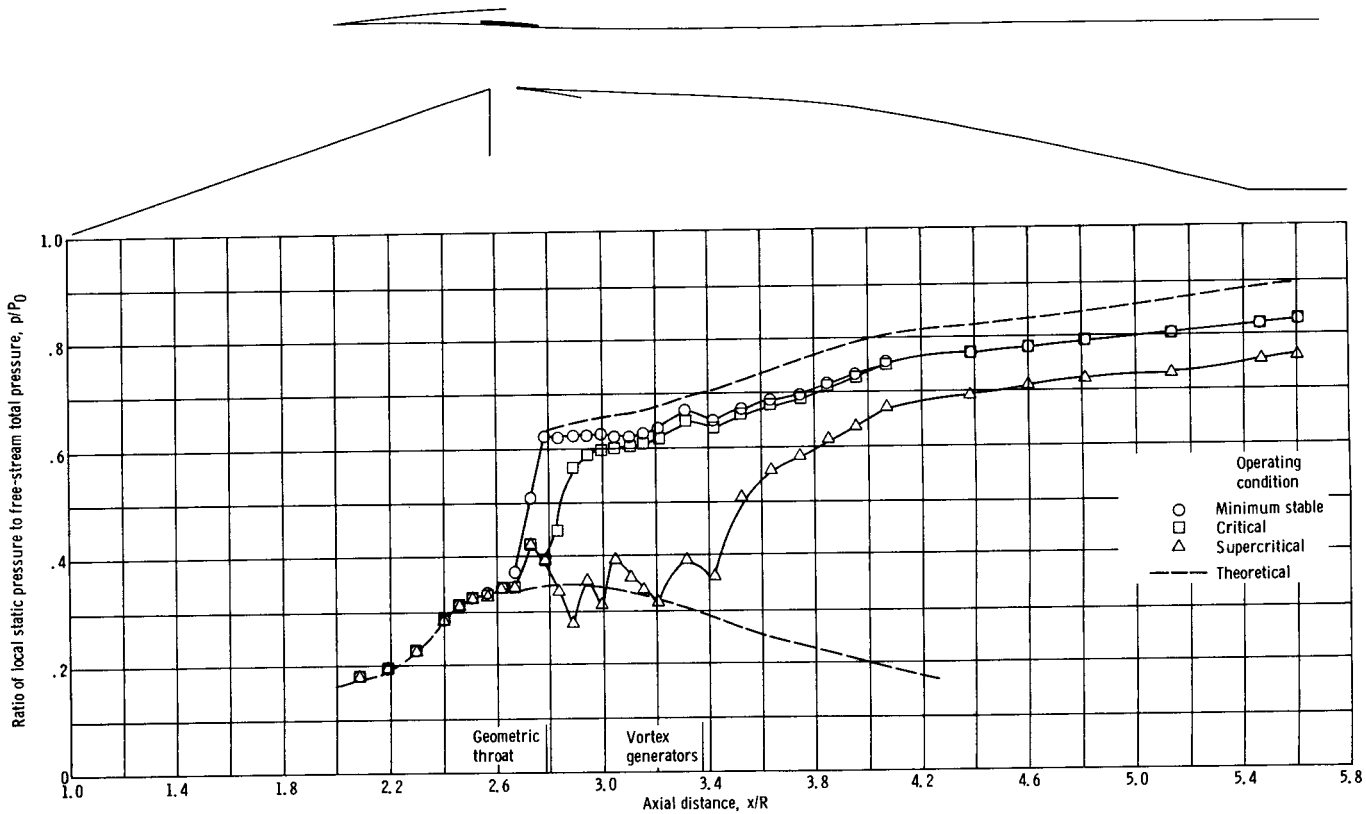


(a) Internal cowl-surface static pressure distributions.

Figure 20. - Diffuser performance for configuration IIIAccb. Free-stream Mach number, $M_0$, 2.5; angle of attack, $\alpha$, $0^0$; cowl-lip position parameter, $\theta_t$, $26.4^0$; bypass mass flow ratio, $m_{by}/m_0$, 0.05.

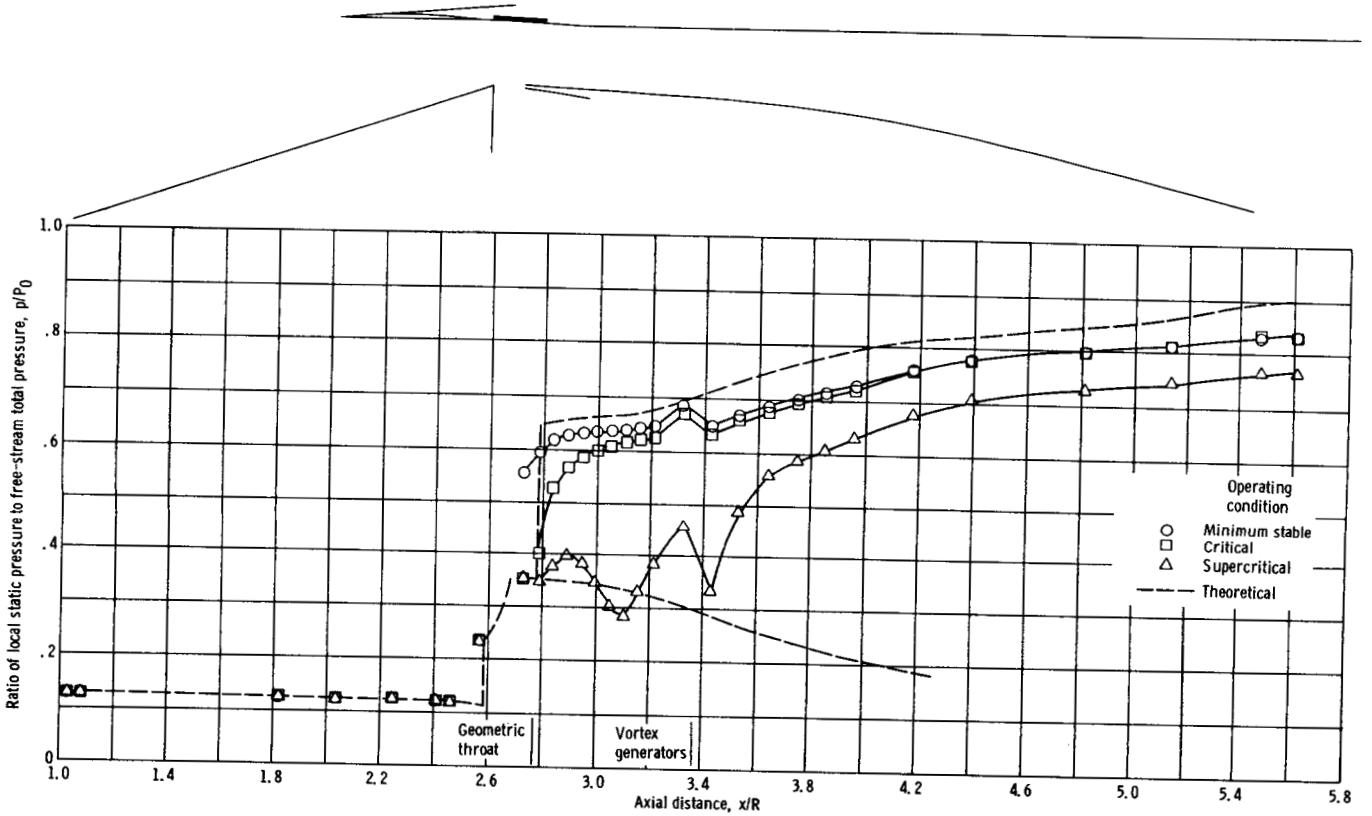


(b) Centerbody-surface static pressure distributions.

Figure 20. - Continued.

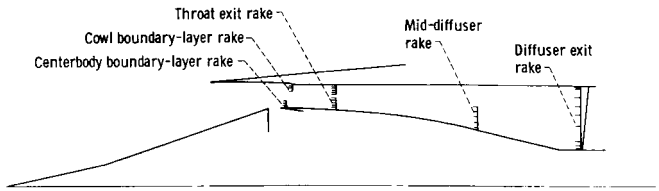


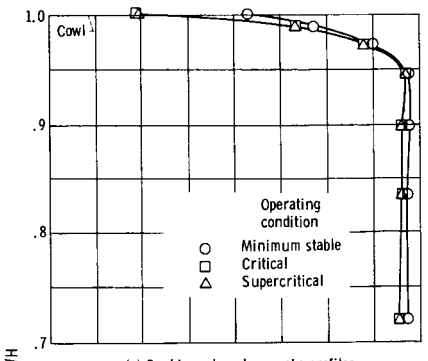


(c) Cowl boundary-layer rake profiles.

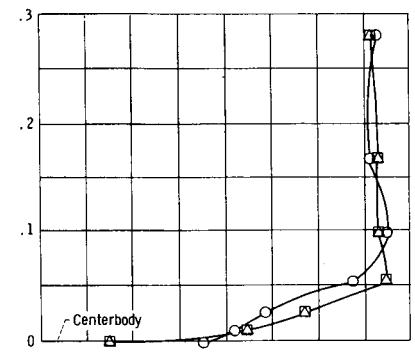


(d) Centerbody boundary-layer rake profiles.

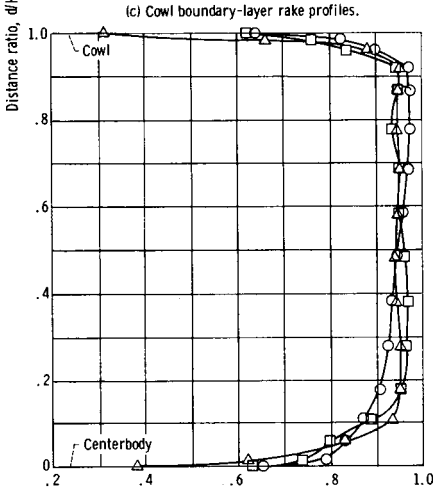


(e) Throat exit rake profiles.

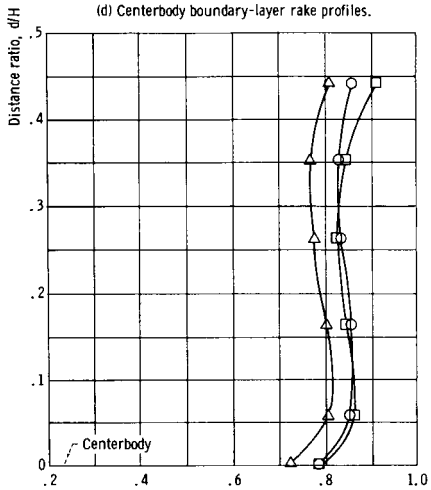


(f) Mid-diffuser rake profiles.

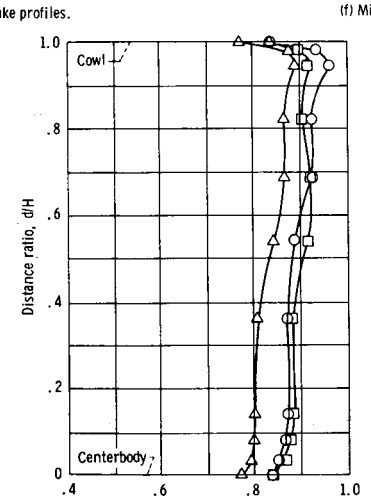


(g) Diffuser exit rake 1 profiles.

Figure 20. - Concluded.

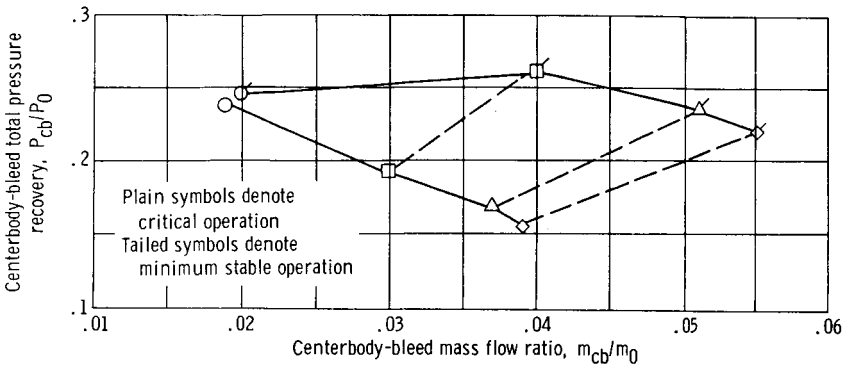


(a) Centerbody-bleed performance.

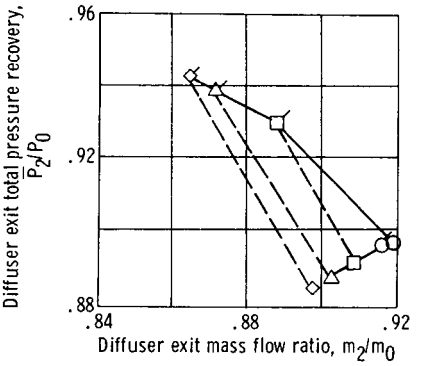


(b) Diffuser performance.

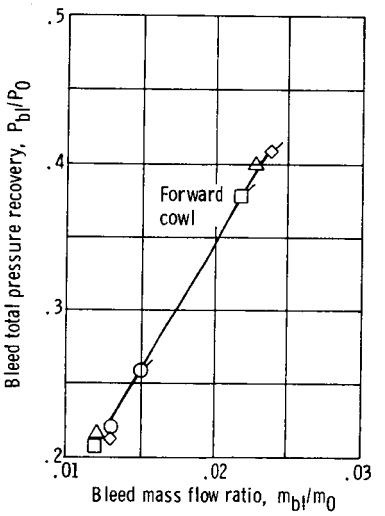


(c) Cowl-bleed performance.

Figure 21. - Stability performance for configuration IIIAccb. Free-stream Mach number, $M_0$, 2.5; angle of attack, $\alpha$, $0^o$; cowl-lip position parameter, $\theta_l$, $26.4^o$; bypass mass flow ratio, $m_{by}/m_0$, 0.05.

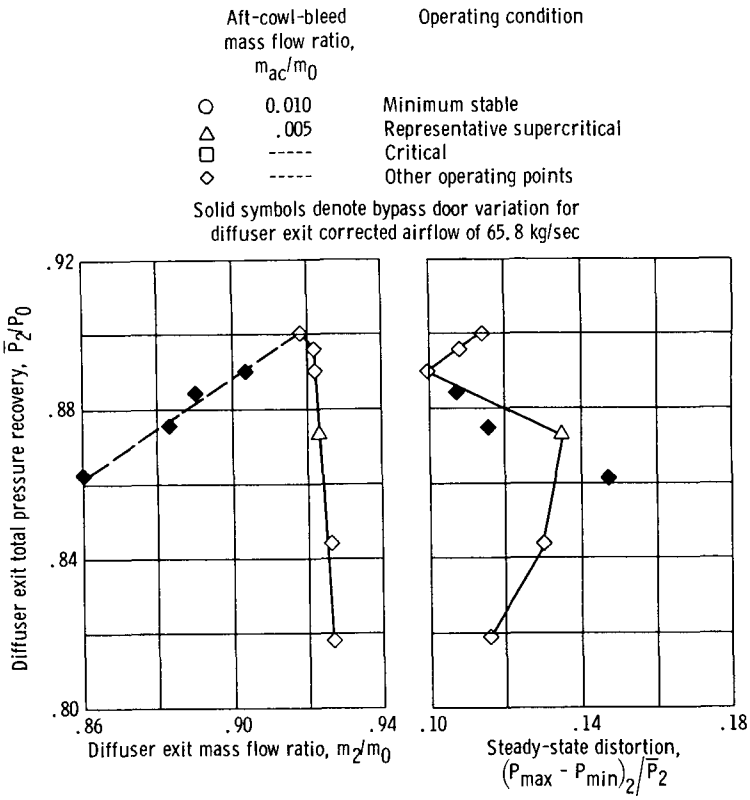


Figure 22. - Steady-state performance for configuration IVAccb. Free-stream Mach number, $M_0$, 2.5; angle of attack, $\alpha$, $0^0$; cowl-lip position parameter, $\theta_l$, $26.4^0$; bypass mass flow ratio, $m_{by}/m_0$, 0.04; forward-cowl-bleed mass flow ratio, $m_{fc}/m_0$, 0.008; centerbody-bleed mass flow ratio, $m_{cb}/m_0$, 0.021.

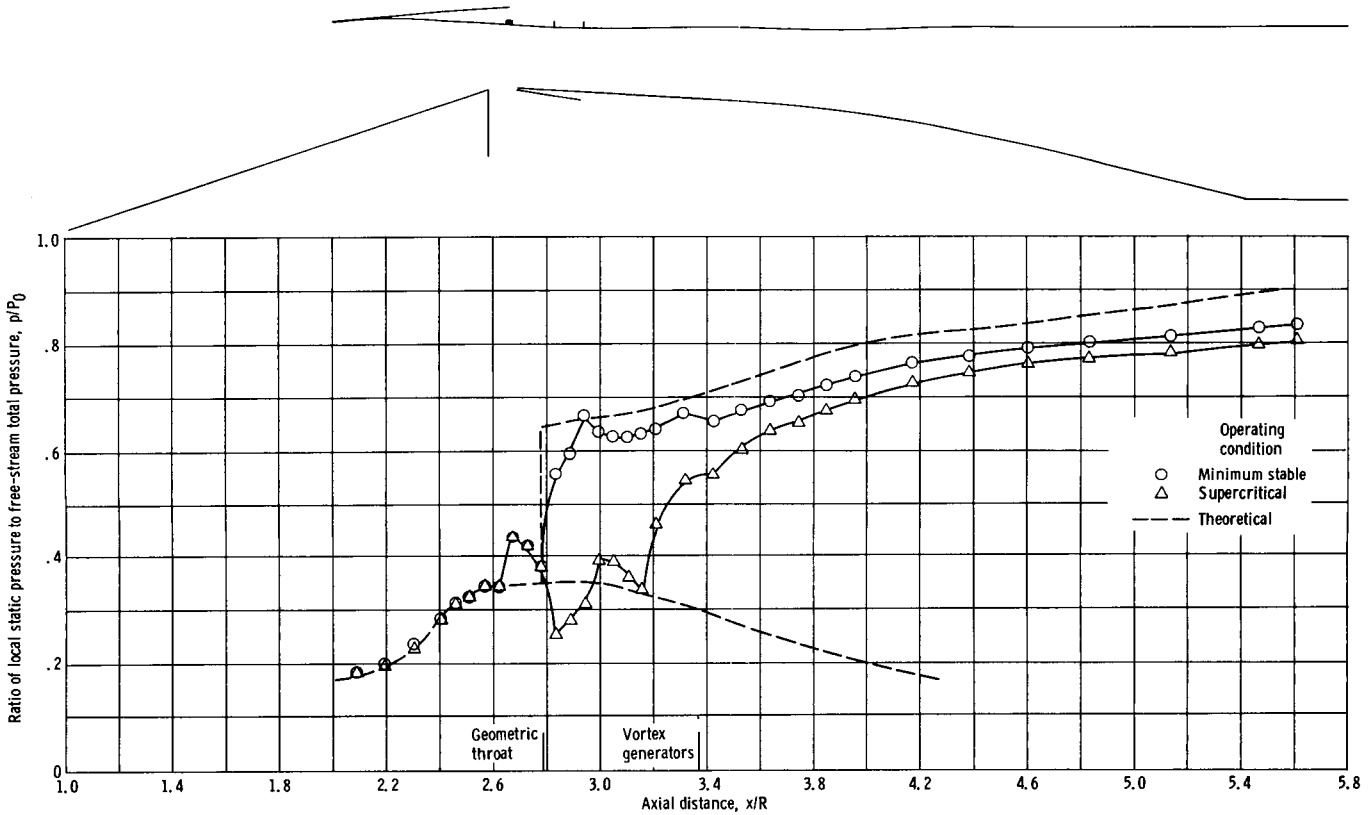


(a) Internal cowl-surface static pressure distributions.

Figure 23. - Diffuser performance for configuration IVAccb. Free-stream Mach number, $M_0$, 2.5; angle of attack, $\alpha$, $0^\circ$; cowl-lip position parameter, $\theta_l$, $26.4^\circ$; bypass mass flow ratio, $m_{by}/m_0$, 0.04.

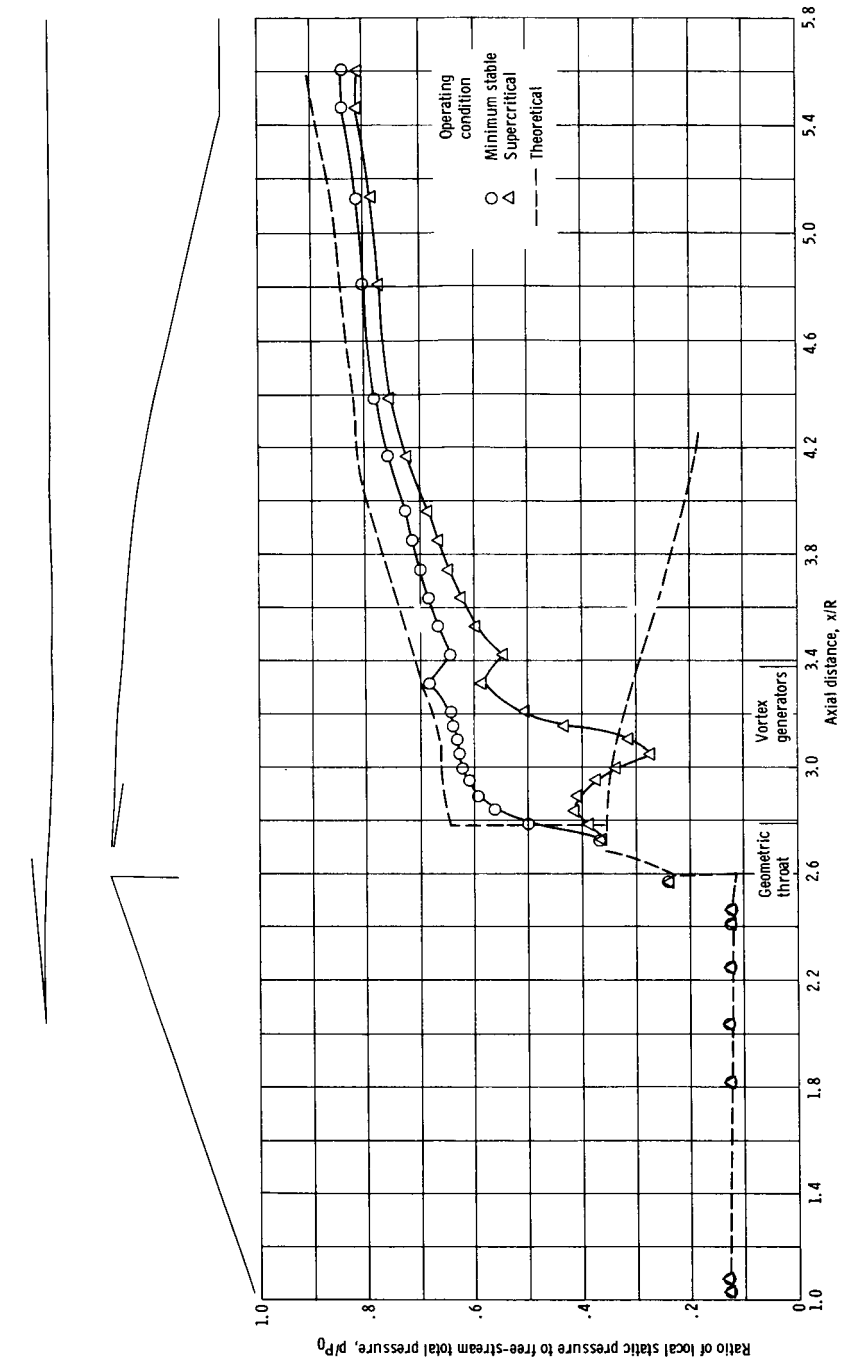


(b) Centerbody-surface static pressure distributions.

Figure 23. - Continued.

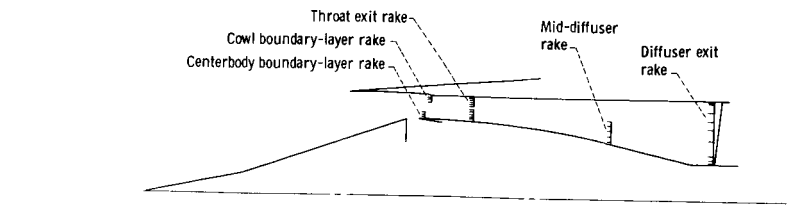


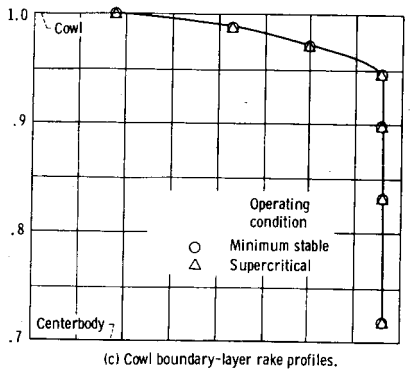


(c) Cowl boundary-layer rake profiles.

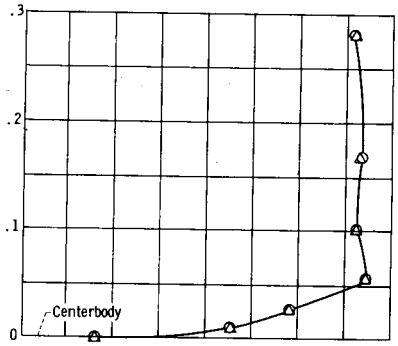


(d) Centerbody boundary-layer rake profiles.

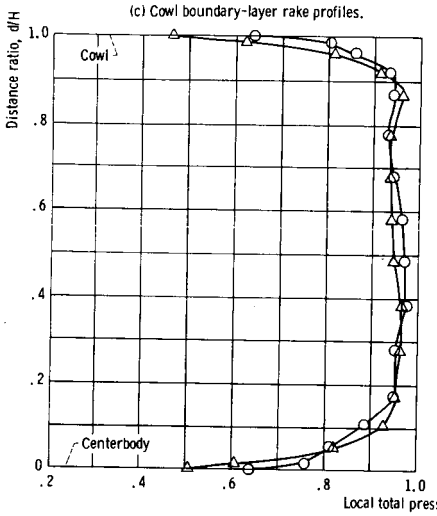


(e) Throat exit rake profiles.

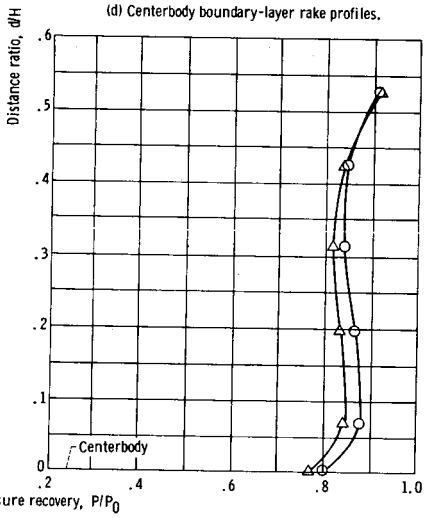


(f) Mid-diffuser rake profiles.

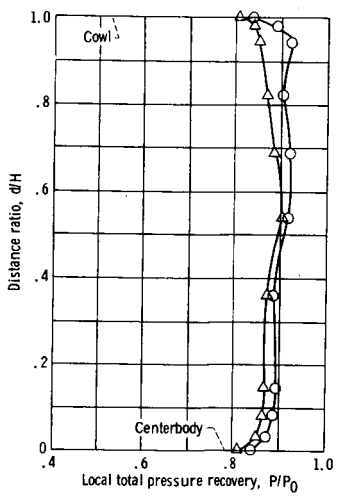


(g) Diffuser exit rake 1 profiles.

Figure 23. - Concluded.

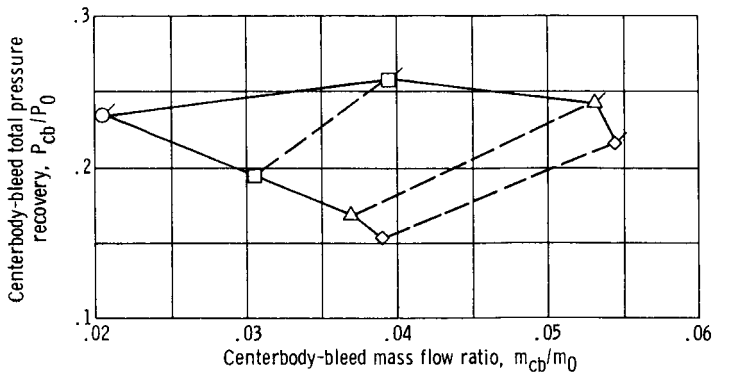


(a) Centerbody-bleed performance.

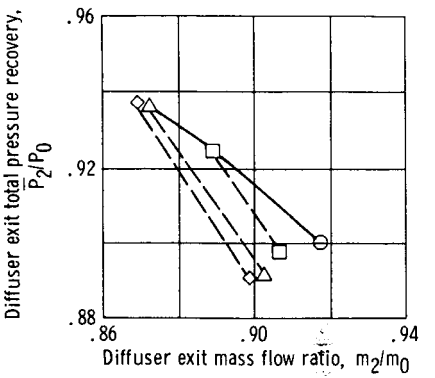


(b) Diffuser performance.

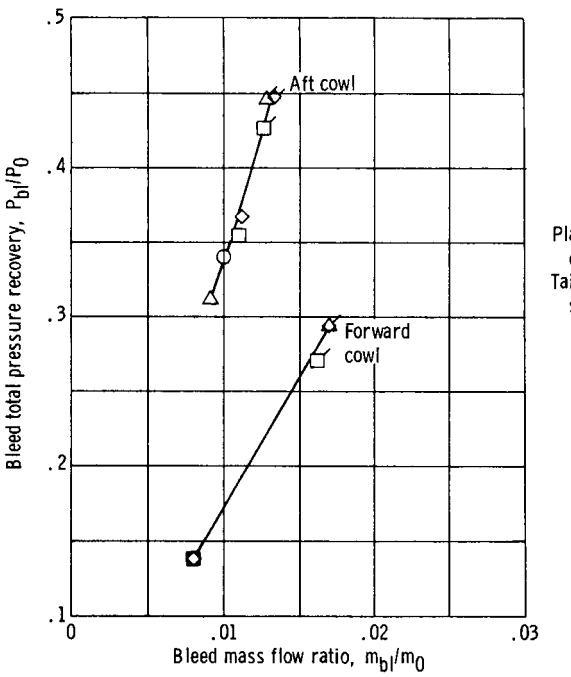


Plain symbols denote critical operation
Tailed symbols denote minimum stable operation

(c) Cowl-bleed performance.

Figure 24. - Stability performance for configuration IVAccb. Free-stream Mach number, $M_0$, 2.5; angle of attack, $\alpha$, $0^o$; cowl-lip position parameter, $\theta_l$, $26.4^o$; bypass mass flow ratio, $m_{by}/m_0$, 0.04.

| | Centerbody-bleed mass flow ratio, $m_{cb}/m_0$ | Forward-cowl-bleed mass flow ratio, $m_{fc}/m_0$ | Aft-cowl-bleed mass flow ratio, $m_{ac}/m_0$ | Operating condition |
|---|---|---|---|---|
| ○ | 0.023 | 0.014 | 0.013 | Minimum stable |
| □ | .022 | .014 | .013 | Critical |
| △ | .021 | .013 | .005 | Representative supercritical |
| ◇ | ----- | ----- | ----- | Other operating points |

Solid symbols denote bypass door variation for diffuser corrected airflow of 65.8 kg/sec

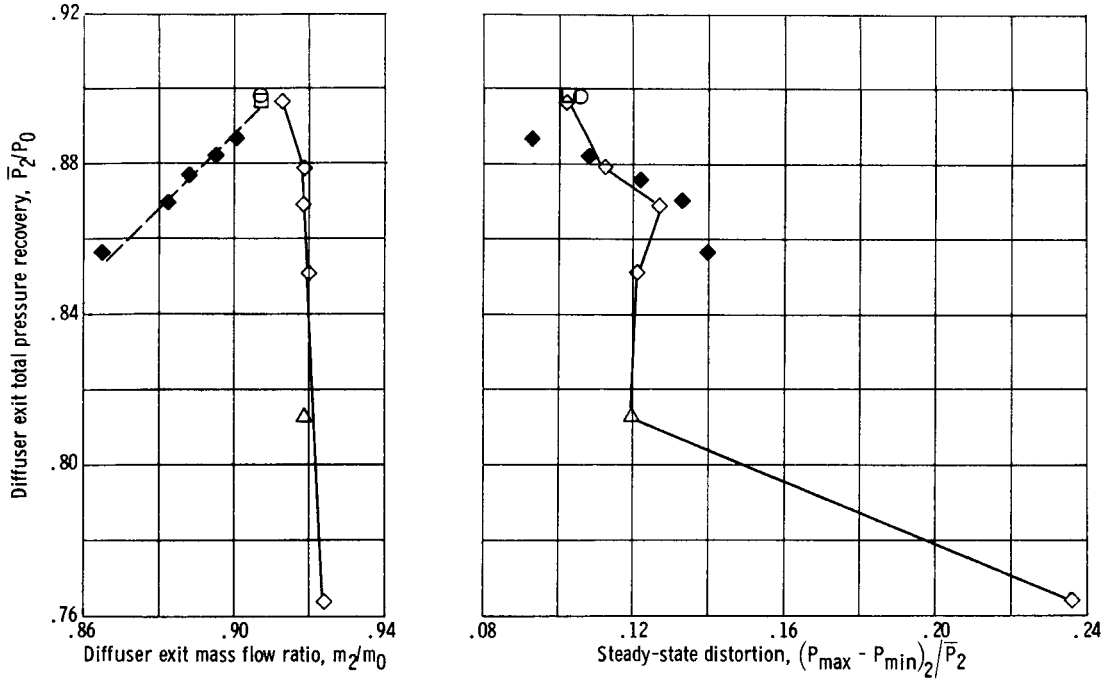


Figure 25. - Steady-state performance for configuration IAccb. Free-stream Mach number, $M_0$, 2.5; angle of attack, $\alpha$, $0^0$; cowl-lip position parameter, $\theta_t$, $26.4^0$; bypass mass flow ratio, $m_{by}/m_0$, 0.03.

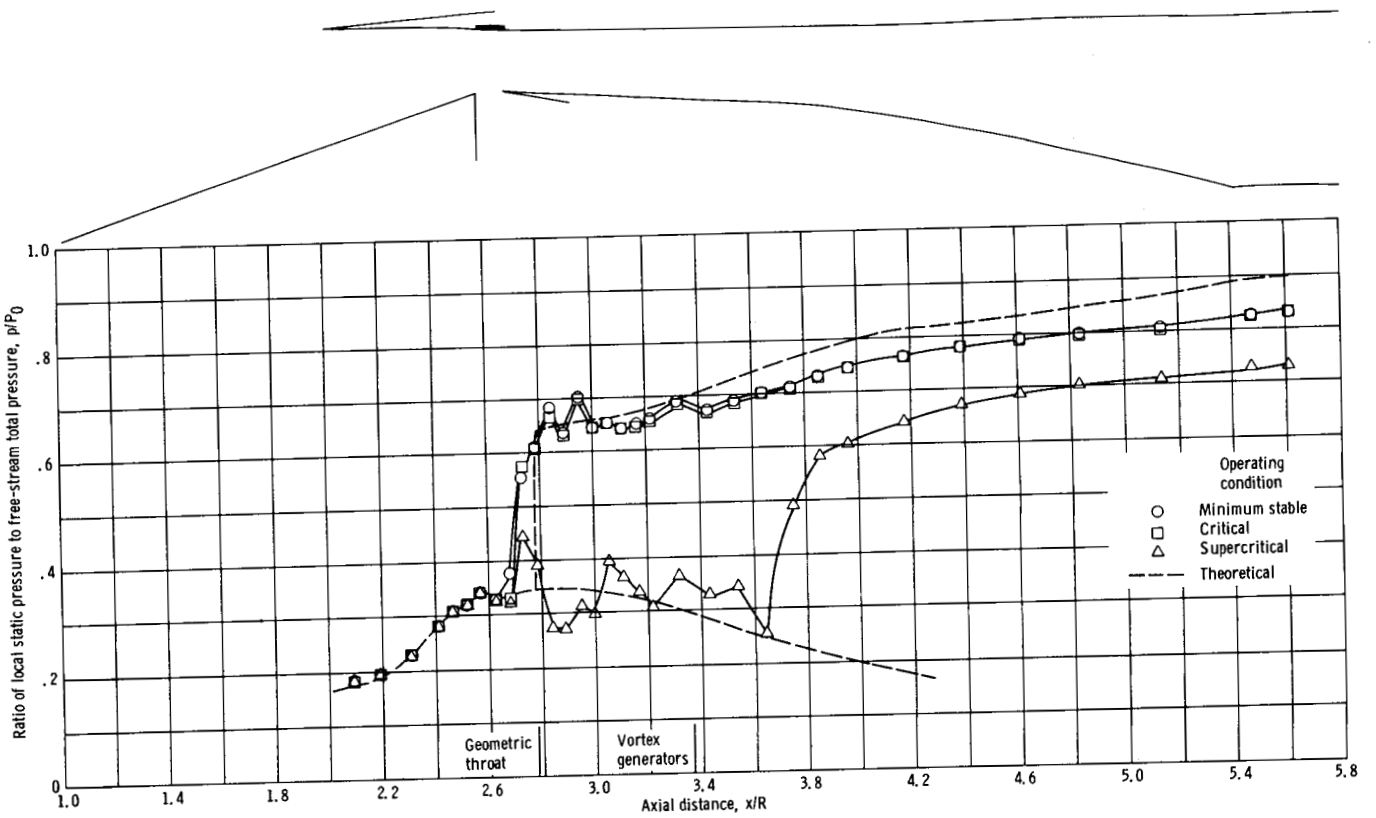


(a) Internal cowl-surface static pressure distributions.

Figure 26. - Diffuser performance for configuration IAccb. Free-stream Mach number, $M_0$, 2.5; angle of attack, $\alpha$, $0^0$; cowl-lip position parameter, $\theta_t$, $26.4^0$; bypass mass flow ratio, $m_{by}/m_0$, 0.03.

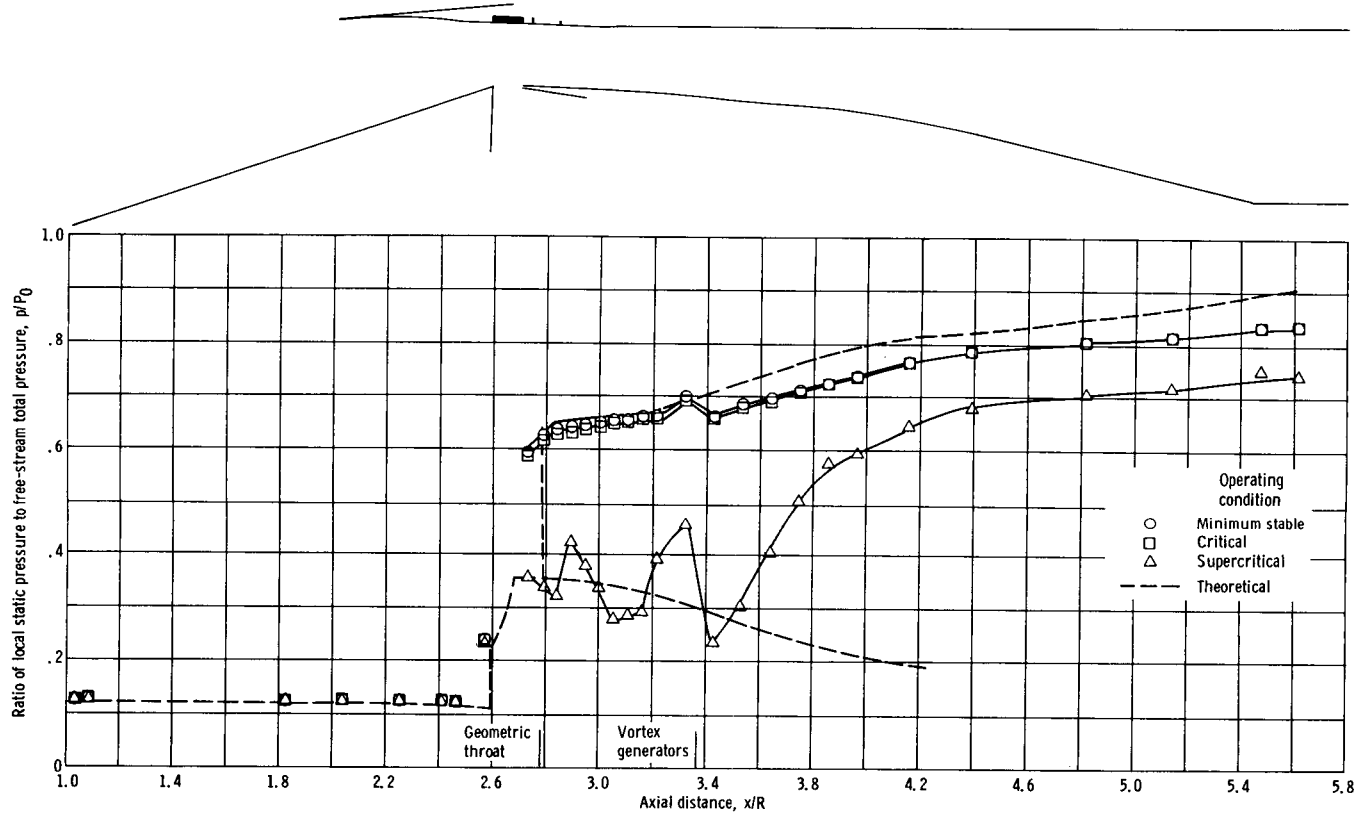


(b) Centerbody-surface static pressure distributions.

Figure 26. - Continued.

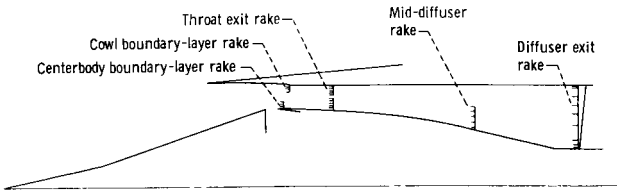


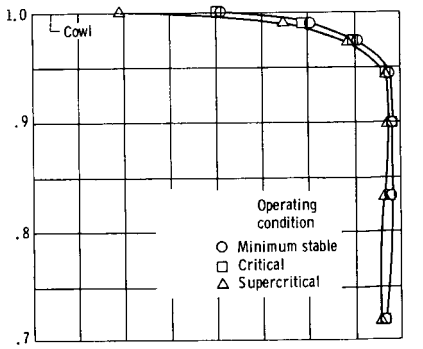


(c) Cowl boundary-layer rake profiles.

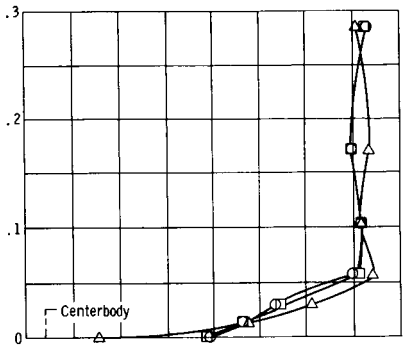


(d) Centerbody boundary-layer rake profiles.

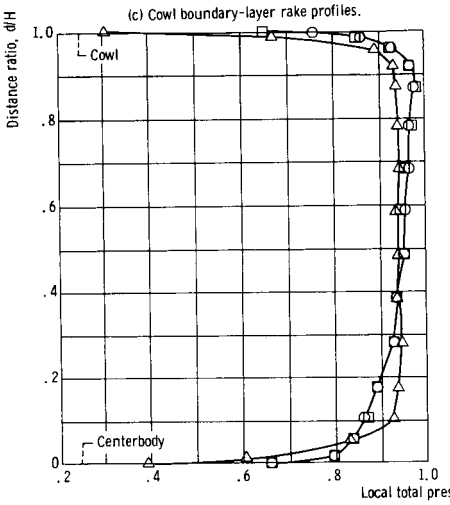


(e) Throat exit rake profiles.

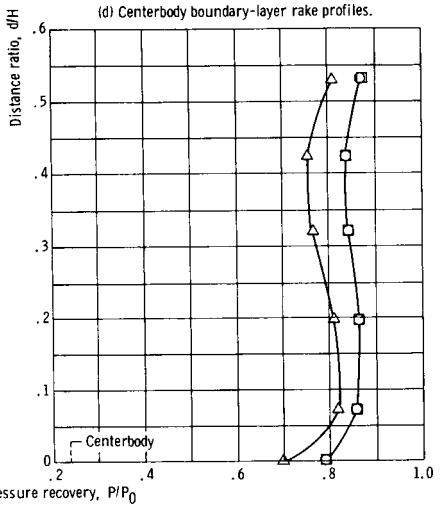


(f) Mid-diffuser rake profiles.

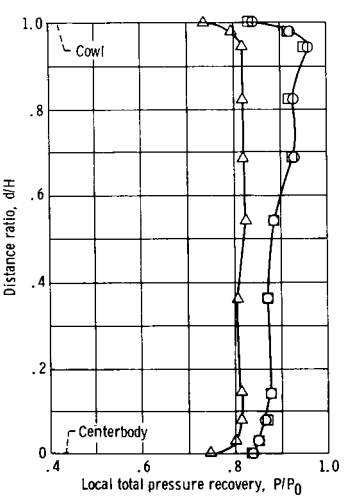


(g) Diffuser exit rake 1 profiles.

Figure 26. - Concluded.

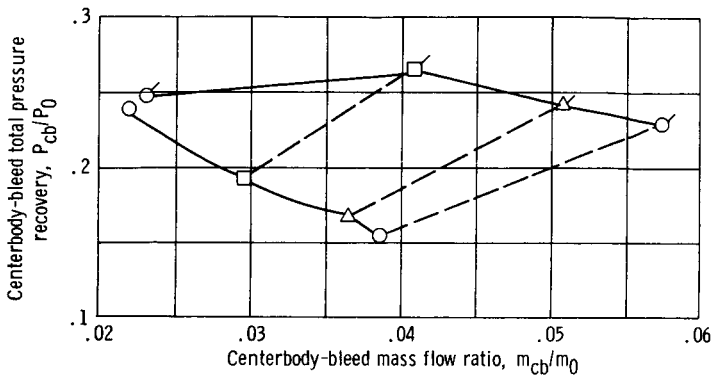


(a) Centerbody-bleed performance.

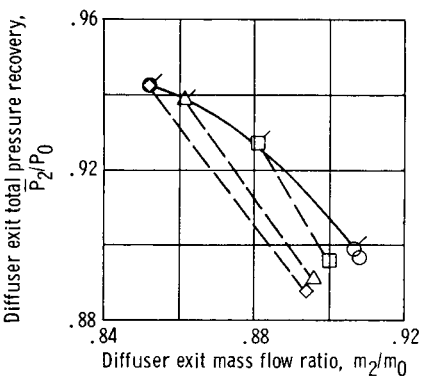


(b) Diffuser performance.

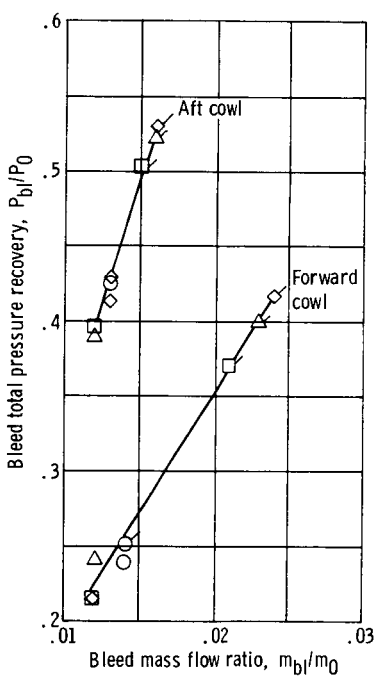


(c) Cowl-bleed performance.

Plain symbols denote critical operation
Tailed symbols denote minimum stable operation

Figure 27. - Stability performance for configuration IAccb. Free-stream Mach number, $M_0$, 2.5; angle of attack, $\alpha$, $0^o$; cowl-lip position parameter, $\theta_l$, $26.4^o$; bypass mass flow ratio, $m_{by}/m_0$, 0.03.

| | Centerbody-bleed mass flow ratio, $m_{cb}/m_0$ | Forward-cowl-bleed mass flow ratio, $m_{fc}/m_0$ | Aft-cowl-bleed mass flow ratio, $m_{ac}/m_0$ | Operating condition |
|---|---|---|---|---|
| ○ | 0.023 | 0.019 | 0.013 | Minimum stable |
| □ | .021 | .017 | .012 | Critical |
| △ | .021 | .017 | .015 | Representative supercritical |
| ◇ | ----- | ----- | ----- | Other operating points |

Solid symbols denote bypass door operation for diffuser corrected airflow of 65.8 kg/sec

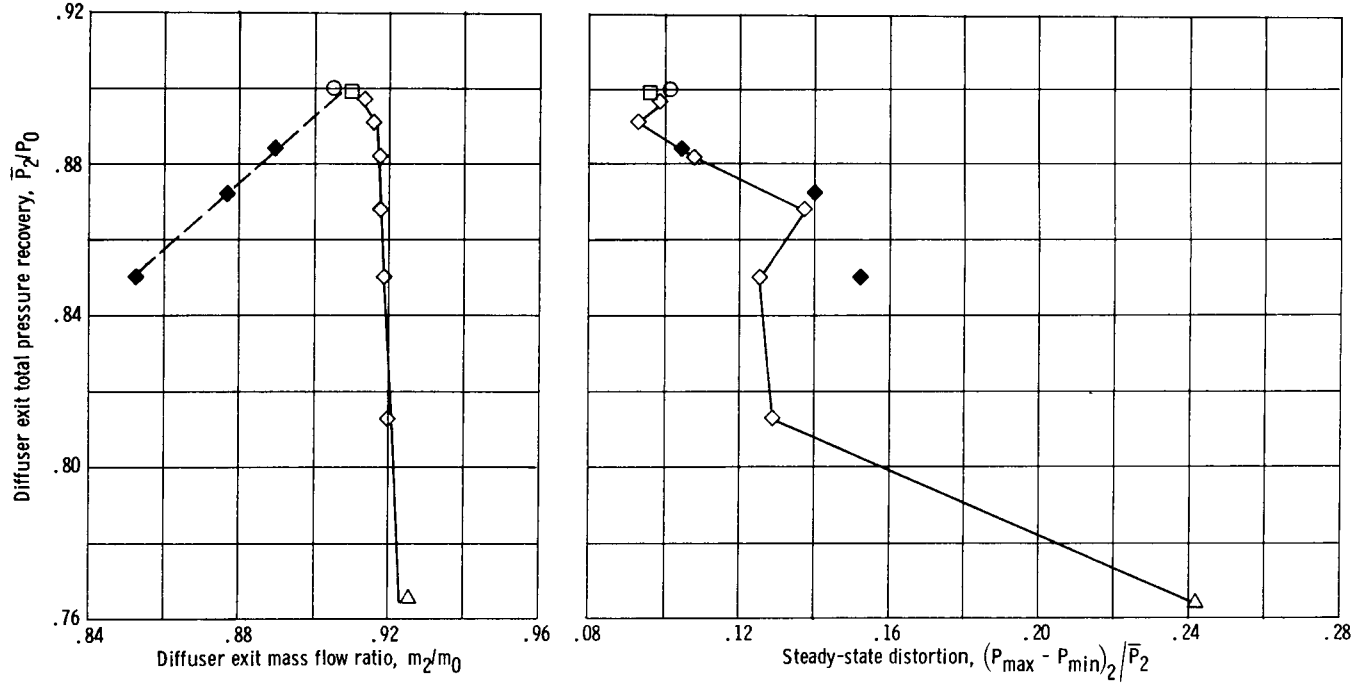


Figure 28. - Steady-state performance of configuration IIAccb. Free-stream Mach number, 2.5; angle of attack, $\alpha$, $0^0$; cowl-lip position parameter, $\theta_t$, $26.4^0$; bypass mass flow ratio, $m_{by}/m_0$, 0.03.

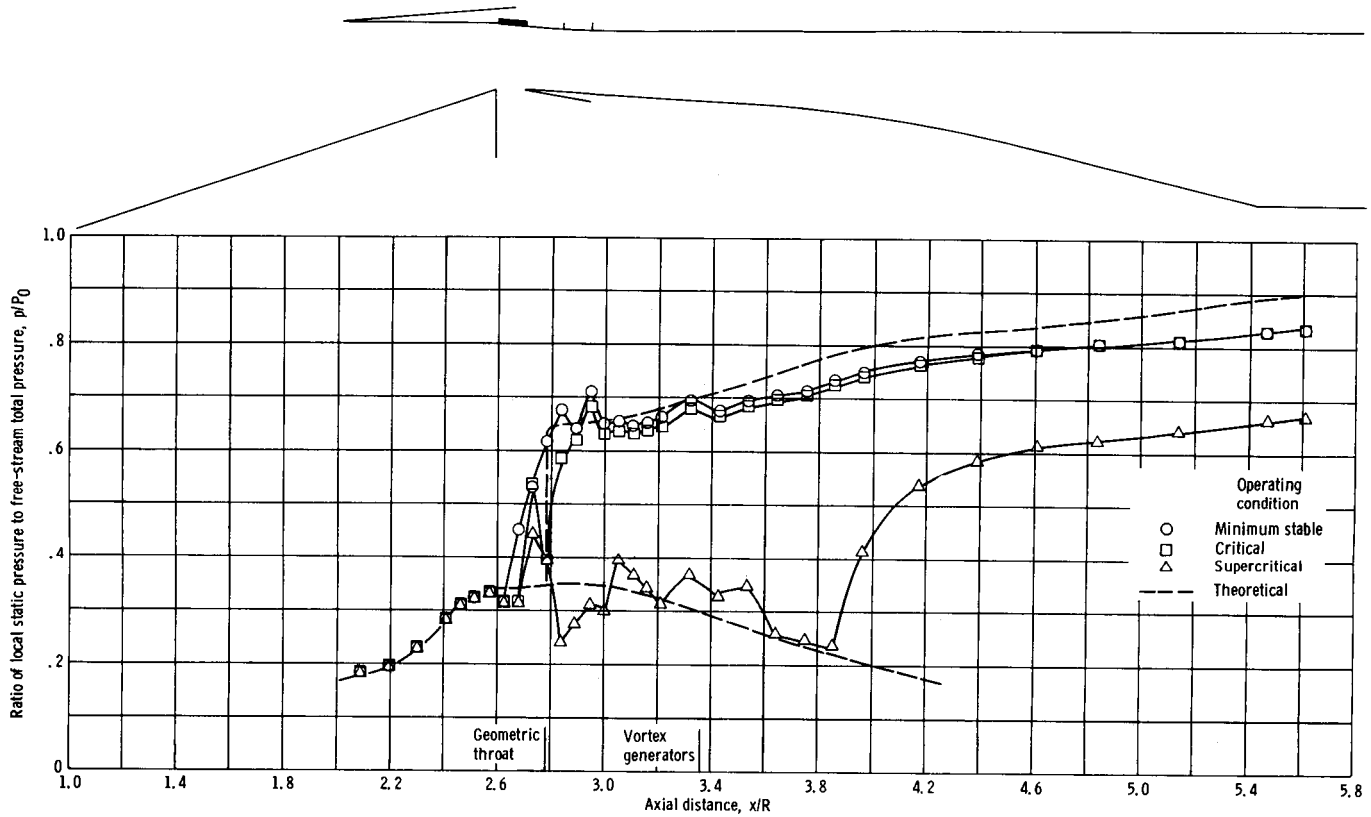


(a) Internal cowl-surface static pressure distributions.

Figure 29. - Diffuser performance for configuration IIAccb. Free-stream Mach number, $M_0$, 2.5; angle of attack, $\alpha$, $0^0$; cowl-lip position parameter, $\theta_t$, $26.4^0$; bypass mass flow ratio, $m_{by}/m_0$, 0.03.

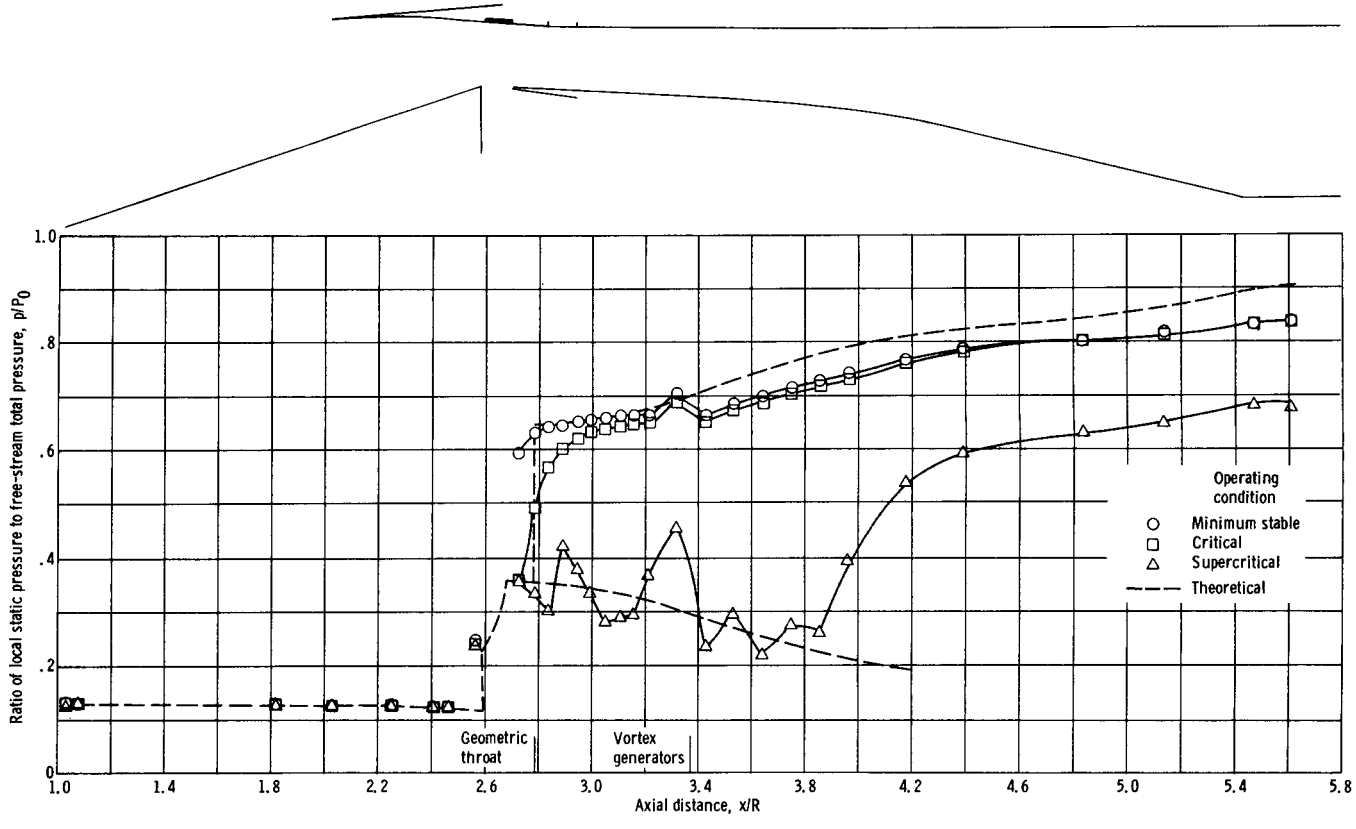


(b) Centerbody-surface static pressure distributions.

Figure 29. - Continued.

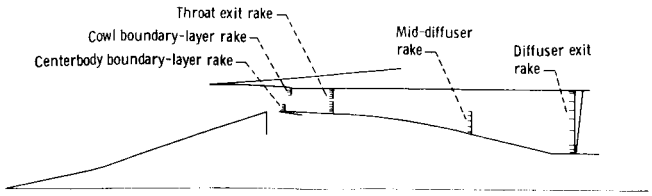


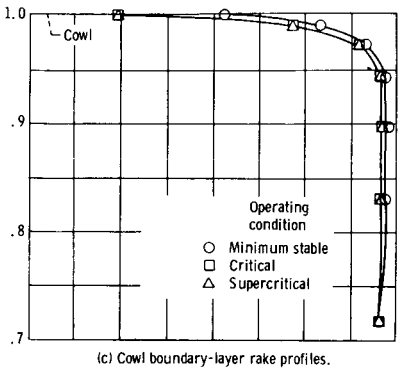


(c) Cowl boundary-layer rake profiles.

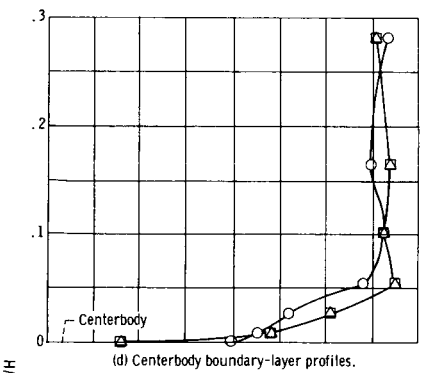


(d) Centerbody boundary-layer profiles.

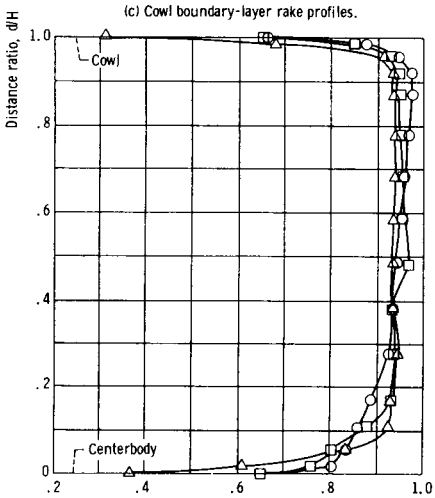


(e) Throat exit rake profiles.

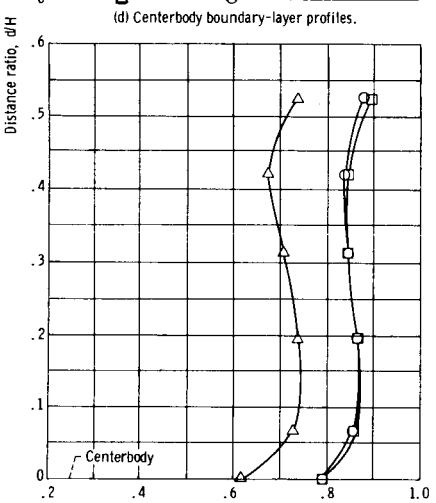


(f) Mid-diffuser rake profiles.

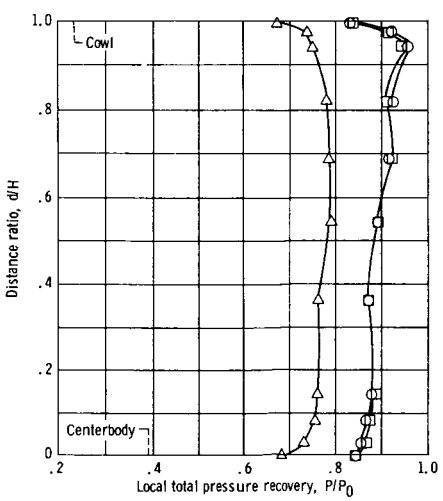


(g) Diffuser exit rake 1 profiles.

Figure 29. - Concluded.

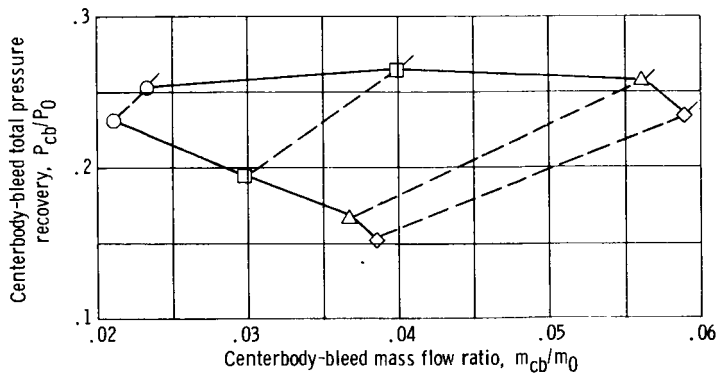


(a) Centerbody-bleed performance.

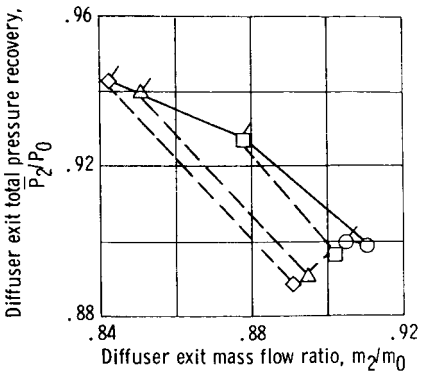


(b) Diffuser performance.

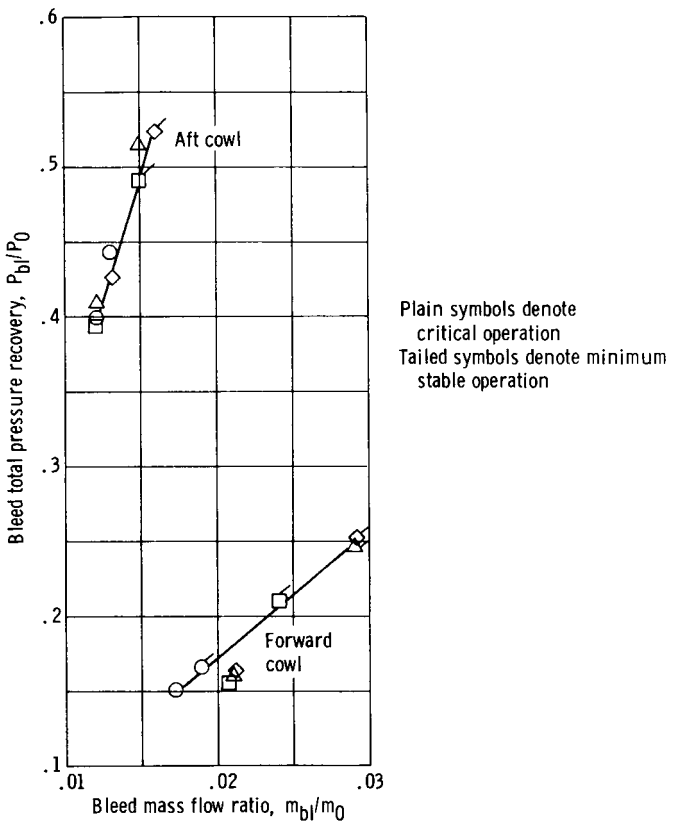


(c) Cowl-bleed performance.

Figure 30. - Stability performance for configuration IIAccb. Free-stream Mach number, $M_0$, 2.5; angle of attack, $\alpha$, $0^0$; cowl-lip position parameter, $\theta_l$, 26.4; bypass mass flow ratio, $m_{by}/m_0$, 0.03.

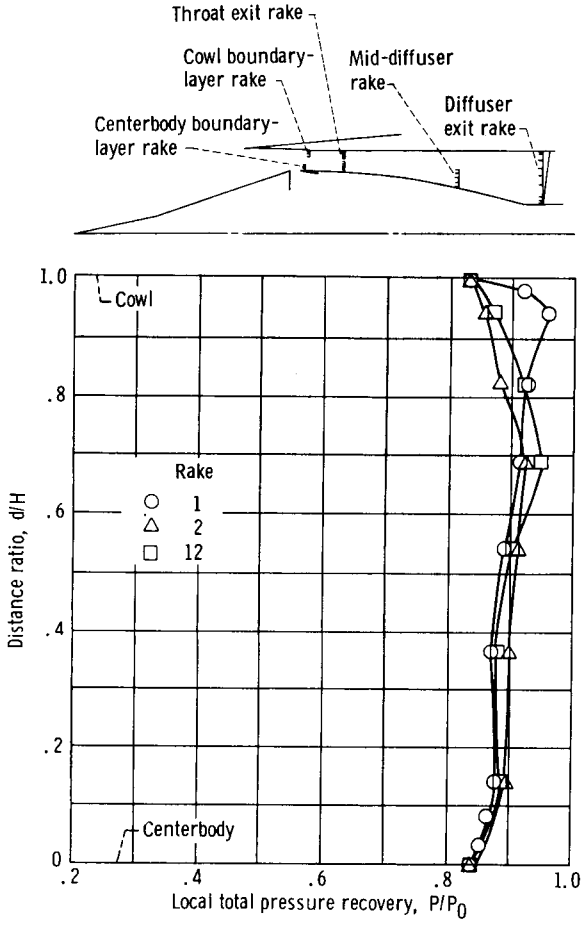


Figure 31. - Diffuser exit rake profiles for configuration IVAccb, minimum stable operating condition. Diffuser exit total pressure recovery, $\bar{P}_2/P_0$, 0.900; centerbody-bleed mass flow ratio, $m_{cb}/m_0$, 0.021; forward-cowl-bleed mass flow ratio, $m_{fc}/m_0$, 0.008; aft-cowl-bleed mass flow ratio, $m_{ac}/m_0$, 0.010; bypass mass flow ratio, $m_{by}/m_0$, 0.04.

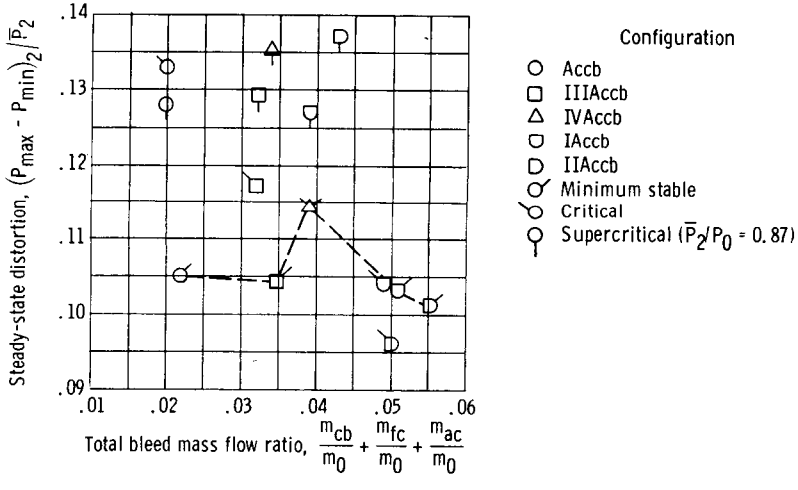


Figure 32. - Steady-state distortion as function of total bleed mass flow.

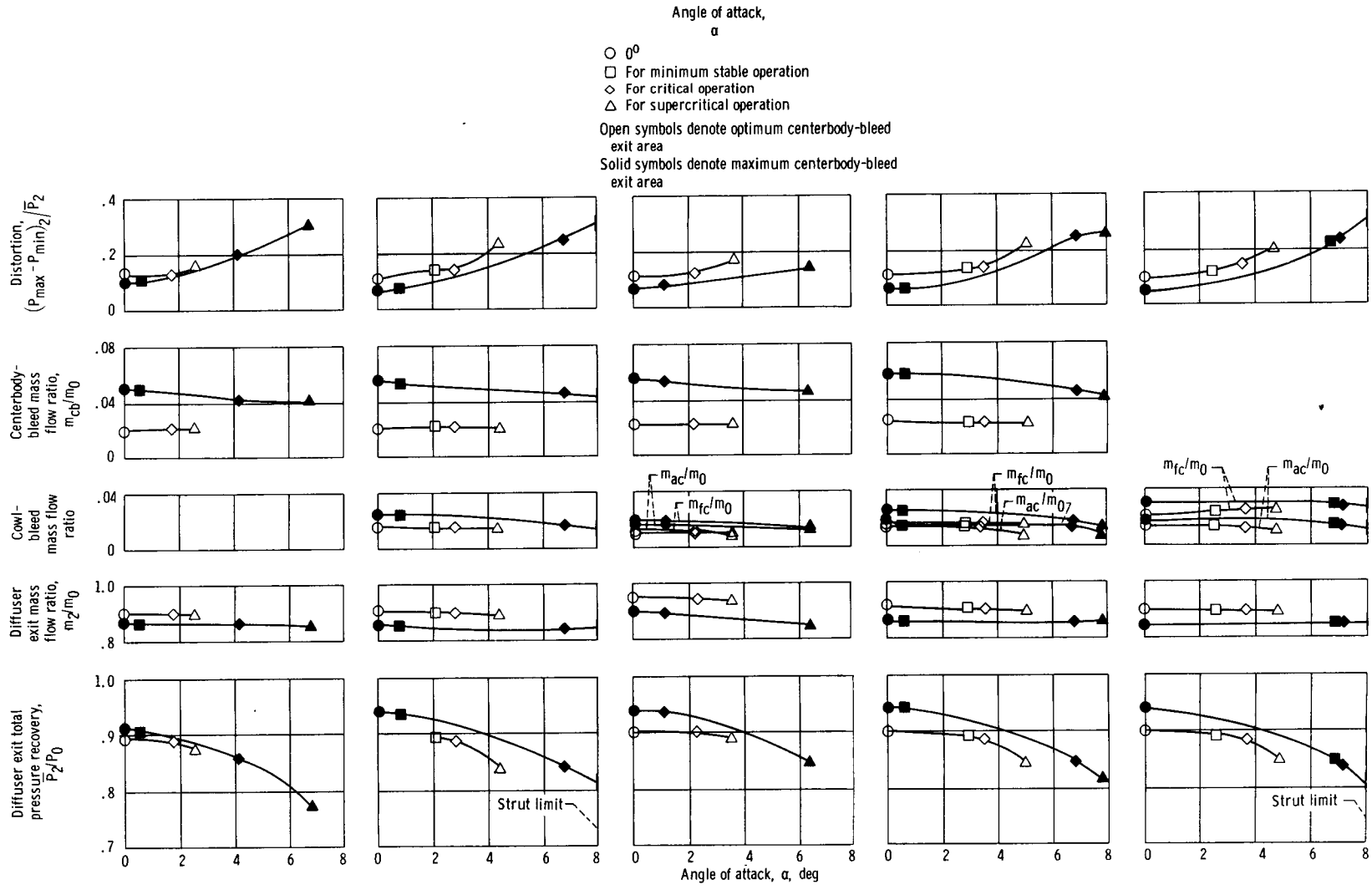


Figure 33. - Angle-of-attack performance.